Chapter 2

The tool: An atmosphere-ocean general circulation model coupled to a Greenland ice-sheet model

To study the evolution of the climate over the 21st century, simulations have been performed with an atmosphere-ocean general circulation model (AOGCM) called LMD5-CLIO2. The atmosphere, the ocean and sea ice are the main constituents of this model. The atmospheric general circulation model is LMD5, originating from the Laboratoire de Météorologie Dynamique (LMD) in Paris. The oceanic general circulation model is CLIO2, developed at the Institut d'Astronomie et de Géophysique G. Lemaître at the UCL. It includes a sea-ice component. The terrestrial biosphere, the soil hydrology and continental snow and ice sheet are roughly parameterized. Consequently, to estimate the impact of the Greenland ice sheet on the 21st century climate, a comprehensive Greenland ice sheet model (GISM) has been coupled with LMD5-CLIO2. This model has been provided by the Vrije Universiteit Brussel. Data between LMD5 and CLIO2 are exchanged and interpolated by a coupler developed at the UCL by *Grenier* [1995] and improved for this thesis work. This coupler is a program based on PVM (Parallel Virtual Machines). Furthermore, a script has been developed during this thesis to orchestrate the synchronization and the transfers of information between LMD5-CLIO2 and GISM.

At the beginning of this thesis, a version of LMD5-CLIO had already been coupled and used to study processes involved in the initial drift (*Grenier* [1995], *Grenier* [1997]). Only short simulations of about 5 years had thus been performed. Since then, the model has been improved to reduce the initial drift. One can not get away from this step prior to any long simulations as those achieved here. In collaboration with the LMD, a new version of the radiative scheme has been introduced in the atmospheric model. It takes into account separately each greenhouse gas and it allows various cloud overlappings. LMD scientists also provided us with a new water vapour advection scheme which tends to reduce the heavy rainfall simulated over high topography. Furthermore, the vertical resolution has been improved (15 levels instead of 11). The direct effect of sulphate aerosols on radiation has been introduced through modifications of the surface albedo. Other parameters involved in physical parameterizations (e.g. the cloud droplet effective radius, the width of the water statistical distribution within a grid cell) have also been tuned to improve the LMD5-CLIO2 results. Each of these changes has been tested in coupled mode in short sensitivity experiments. Those simulations are not shown but the selected values for the parameters are given. Similarly, CLIO has been adapted to reduce the coupled model drift. A new version CLIO2 has been adopted as it contains an improved version of vertical mixing parameterization. The new topography with an open passage between Greenland and America has also been chosen. It implies modification of the surface mask in the atmospheric model and changes in the interpolation performed by the coupler. Modifications of the sea-ice albedo and of the snow conductivity have improved the simulated Arctic sea ice. Again, these adaptations have been tested in sensitivity experiments. The last set of developments concerns the coupler. New fields are transfered from CLIO2 to LMD5, namely the sea-ice and ocean albedos. In the opposite direction, the freshwater flux provided by LMD5 is changed in the coupler to take into account the Greenland runoff and calving computed by GISM.

In the present chapter, three models are described: LMD5, CLIO2 and GISM. The main features of the procedures developed to couple both LMD5 to CLIO2 and LMD5-CLIO2 to GISM are explained. Afterwards, the experimental design of the long-term experiments covering the 21st century is reported. Finally, we depict the control-simulation initial drift.

2.1 The atmosphere-ocean general circulation model

The most relevant climate features for human life and activities are rather the continental surface conditions (like surface air temperature, precipitation, or wind speed) than globally averaged characteristics of the climate system. As we are interested in the characteristics and behaviour of the individual climate system components, we can't consider the climate system as a single box. We must separate the energy stored in the atmosphere, ocean, cryosphere, ..., and introduce interactions between all the components which redistribute energy or species mass between them. But, of course, we can't take everything into account in models. The main limitations are our understanding of the physical processes and computer power.

The more complex tools currently available to study the climate are three-dimensional atmosphere-ocean general circulation models (AOGCM) representing the atmosphere, the ocean, and the sea ice. They are based on physical laws - conservation of momentum, energy, and mass -, and the three space dimensions and time are explicitly taken into account. Spatial and temporal resolutions are more or less coarse depending on the computer power available. Furthermore, some assumptions are made to simplify the system. Due to these two limitations, some processes are not explicitly resolved. The most important ones are parameterized by linking them to variables resolved by the model.

The AOGCM used for this work is made up of two programs: an Atmospheric General Circulation Model (AGCM) developed at the Laboratoire de Météorologie Dynamique (LMD) in Paris, and an Oceanic General Circulation Model (OGCM) developed at the UCL. More precisely, the atmospheric component is based on LMD5.2, and the oceanic and sea-ice component is CLIO2.0. Our AOGCM is called hereafter LMD5-CLIO2. Furthermore, as the surface of the ocean or sea ice is also the base of the atmosphere, boundary conditions are exchanged between the AGCM and the OGCM. No correction is applied during this transfer to help keeping the modeled climate close to observations. The model is totally free, the only forcing is the solar energy arriving at the top of the atmosphere.

2.1.1 Physical equations and assumptions in the model components

2.1.1.1 Horizontal momentum equation

Holton [1992] applies **Newton's second law** to a geophysical fluid. It is assumed that the ocean or the atmosphere are thin layers over the Earth's solid surface, and thus the distance from the studied point and the Earth center is constant and equal to the Earth's radius. After a scale analysis, Newton's second law leads to the following equation for the horizontal velocity $\overrightarrow{u}$:

$$\frac{\partial \overrightarrow{u}}{\partial t} + \left(\overrightarrow{u} \cdot \overrightarrow{\nabla_h}\right) \overrightarrow{u} + w \frac{\partial \overrightarrow{u}}{\partial z} = -f \overrightarrow{e_z} \times \overrightarrow{u} - \frac{1}{\rho} \overrightarrow{\nabla_h} p + \overrightarrow{F_{int}} + \overrightarrow{\tau},$$

where w, ρ, p are the vertical velocity, the density, and the pressure, respectively. The Coriolis factor $f = 2\Omega \sin(\varphi)$ depends on the angular speed of the Earth's rotation Ω and on latitude φ. (x, y, z) are the horizontal and vertical coordinates, and $\overrightarrow{e_z}$ is a vertical unit vector. $\overrightarrow{\nabla_h} = \left(\frac{\partial}{\partial x}, \frac{\partial}{\partial y}\right)$. This equation indicates that the evolution of the horizontal velocity is influenced by the Coriolis force, the pressure force, the internal force $\overrightarrow{F_{int}}$, and the friction at the boundaries $\overrightarrow{\tau}$.

A scale analysis on the vertical momentum equation (see *Holton* [1992]) leads to the hydrostatic approximation:

$$\frac{\partial p}{\partial z} = -\rho g,$$

which means that the pressure at any point is simply equal to the weight of a unit cross-section column above that point.

CLIO2 uses the Boussinesq approximation in the **ocean**. This approximation states that the variation of the density are small compared to its mean, $\rho = \rho_0$. It allows to replace the density by its reference value ρ_0, except in the expression of gravitational force. Thus, the momentum equations become:

$$\frac{\partial \overrightarrow{u}}{\partial t} + \left(\overrightarrow{u} \cdot \overrightarrow{\nabla_h}\right) \overrightarrow{u} + w \frac{\partial \overrightarrow{u}}{\partial z} = -f \overrightarrow{e_z} \times \overrightarrow{u} - \frac{1}{\rho_0} \overrightarrow{\nabla_h} p + \overrightarrow{F_{int}} + \overrightarrow{\tau},$$

and

$$\frac{\partial p}{\partial z} = -\rho g.$$

The internal force is obtained using kinematic viscosity coefficients κ_h and κ_z:

$$\overrightarrow{F_{int}} = \kappa_h \overrightarrow{\nabla_h}^2 \overrightarrow{u} + \frac{\partial}{\partial z} \left(\kappa_z \frac{\partial \overrightarrow{u}}{\partial z}\right).$$

The surface friction is determined by subgrid-scale characteristics of the surface; so, it is parameterized in the model (see section 2.1.5).

For the **atmosphere**, the equations are not written using the height as vertical coordinate in LMD5. The vertical levels are defined according to the so-called sigma-coordinate:

$\sigma = \frac{p}{p_s}$ where p_s is the surface pressure. The surface is then easily defined by $\sigma = 1$. *Holton* [1992] re-writes the momentum equations using this coordinate and obtains for the hydrostatic equilibrium:

$$\frac{\partial p}{\partial \sigma} = -\rho \frac{\partial \Phi}{\partial \sigma},$$

where Φ is the geopotential (see chapter 1). The "horizontal" momentum equation becomes:

$$\frac{\partial \overrightarrow{U}}{\partial t} + \left(\overrightarrow{U} \cdot \overrightarrow{\nabla_\sigma}\right) \overrightarrow{U} + \omega \frac{\partial \overrightarrow{U}}{\partial \sigma} = -f \overrightarrow{e_\sigma} \times \overrightarrow{U} - \overrightarrow{\nabla_\sigma} \Phi - \frac{1}{\rho} \overrightarrow{\nabla_\sigma} p + \overrightarrow{F_{int}} + \overrightarrow{\tau}.$$

$\overrightarrow{\nabla_\sigma}$ represents the new horizontal derivatives at a constant sigma level. $\overrightarrow{U}$ and $\omega = \frac{\partial \sigma}{\partial t}$ are the new horizontal and vertical velocities, respectively. $\overrightarrow{e_\sigma}$ is a unit vector perpendicular to the constant sigma level. $-\overrightarrow{\nabla_\sigma}\Phi$ is the component of the gravity force parallel to a constant sigma-level. Dissipation is taken into account by $\overrightarrow{F_{int}}$. A biharmonic operator is applied on the divergence and rotational wind. The planetary boundary layer parameterization computes the vertical dissipation of momentum and the surface stress (see section 2.1.5).

In CLIO2, **sea ice** is considered as a two-dimensional continuum. The general three-dimensional momentum equation described above is integrated through the ice thickness. A horizontal momentum equation is obtained in which the density is replaced by the mass of the snow-ice system m per unit area. Furthermore, sea ice floats over seawater. The sea surface is not flat. Its dynamical elevation η is the difference between its height and its equilibrium height. Similarly to the $-\overrightarrow{\nabla_\sigma}\Phi$ term in the atmospheric model, the component of the gravity force parallel to the sea surface is $-g\overrightarrow{\nabla_{z'}}\eta$, where $\overrightarrow{\nabla_{z'}}$ is the "horizontal" gradient along the sea surface. Finally, scale analysis indicates that the advection of momentum may be neglected (*Fichefet and Morales Maqueda* [1997]). All these considerations leads to the following horizontal momentum equation:

$$m \frac{\partial \overrightarrow{u}}{\partial t} = -mf \overrightarrow{e_z} \times \overrightarrow{u} - mg \overrightarrow{\nabla_h} \eta + \overrightarrow{F_{int}} + \overrightarrow{\tau_{ai}} + \overrightarrow{\tau_{wi}},$$

where $\overrightarrow{\tau_{ai}}$ and $\overrightarrow{\tau_{wi}}$ are the surface force per unit area due to air and water drags and are parameterized (see sections 2.1.5 and 2.1.4). The internal force $\overrightarrow{F_{int}}$ is computed according to *Hibler* [1979]. Sea ice is assumed to be a viscous-plastic continuum.

2.1.1.2 Continuity equation

Holton [1992] develops the continuity equation, which expresses the conservation of mass:

$$\frac{\partial \rho}{\partial t} + \left(\overrightarrow{u} \cdot \overrightarrow{\nabla_h}\right) \rho + \rho \left(\frac{\partial w}{\partial z} + \overrightarrow{\nabla_h} \cdot \overrightarrow{u}\right) = 0.$$

This mathematical relationship is used in **LMD5** but it is re-written using the sigma-coordinate to obtain:

$$\frac{\partial p_s}{\partial t} + \overrightarrow{\nabla_\sigma} \cdot \left(p_s \overrightarrow{U}\right) + p_s \frac{\partial \omega}{\partial \sigma} = 0.$$

The Boussinesq approximation (see above) assumes that the density is constant ($\rho = \rho_0$) as far as it is not associated to gravity. Consequently, the continuity equation used in **CLIO2** is :

$$\frac{\partial w}{\partial z} + \overrightarrow{\nabla_h} \cdot \overrightarrow{u} = 0.$$

In the **sea-ice** component, conservation of mass is handled as any other conservation as thermodynamic source and sink terms must be introduced.

2.1.1.3 Conservation equations

In the atmosphere, as in the ocean or in sea ice, many quantities have to be conserved. One of the most obvious example is energy. The conservation equation of a quantity ψ, expressed in amount per unit volume, must take into account the local variation of the quantity with time, the advection by the velocity field, the variation of the volume, the diffusivity D_ψ, but also the sources or sinks. The sources or sinks may act at the surface F_ψ^{surf} (i.e., at the interface which another medium) or in the volume F_ψ^{vol}. All these terms are handled in the following equation:

$$\frac{\partial \psi}{\partial t} + \overrightarrow{\nabla_h} \cdot (\overrightarrow{u}\psi) = \frac{\partial \psi}{\partial t} + \left(\overrightarrow{u} \cdot \overrightarrow{\nabla_h}\right)\psi + w\frac{\partial \psi}{\partial z} + \psi\left(\frac{\partial w}{\partial z} + \overrightarrow{\nabla_h} \cdot \overrightarrow{u}\right) = D_\psi + F_\psi^{surf} + F_\psi^{vol}.$$

Physical fields are of course advected in the **sea ice** component of CLIO2. These are the ice concentration A, the snow volume per unit area Ah_s, the ice volume per unit area Ah_i, the snow and ice sensible heat contents per unit area AQ_s and AQ_i (with $Q_r = (\rho c_p)_c \int_0^{h_c} T_c(z)dz$ the vertical integral of the temperature time the density and the heat capacity, the subscript c stands either for the ice i or snow s), and the latent heat contained in the brine reservoir per unit area AQ_{st} (More details on these quantities can be found in section 2.1.4). This ensures the conservation of snow and ice masses and of energy. The source and sink terms associated to atmospheric or oceanic heat fluxes, ice or snow melting or accretion, ... are parameterized as described in section 2.1.4. Dissipation is modeled as $D_\psi = \kappa \overrightarrow{\nabla}^2 \psi$.

In **LMD5**, any quantity ε is expressed per unit of mass. The energy is the enthalpy of an air parcel of 1 kg, the specific humidity is the water vapour amount in 1 kg of air, the liquid water content is also expressed in $\frac{\text{kg}_{\text{eau}}}{\text{kg}_{\text{air}}}$. Consequently, $\psi = \rho\varepsilon$ and using the continuity equation, it comes out that:

$$\frac{\partial \varepsilon}{\partial t} + \left(\overrightarrow{U} \cdot \overrightarrow{\nabla_\sigma}\right)\varepsilon + \omega\frac{\partial \varepsilon}{\partial \sigma} = D_\varepsilon + F_\varepsilon^{surf} + F_\varepsilon^{vol}.$$

The LMD's model resolves this equation for the potential temperature, the specific humidity, and the liquid water content. Precipitation and condensation are volume source or sink of vapour or liquid water. Evaporation is a surface source of water vapour. For temperature, volume source and sink are parameterized in the radiative scheme; the condensation scheme and the surface fluxes act as surface source or sink. All these parameterizations are briefly described below (see section 2.1.5). Horizontal diffusion is applied to potential enthalpy, via a biharmonic operator. Because of the highly diffusive character of the flux-form water vapour tendency equation, no further horizontal diffusion of specific humidity and liquid water content is included. Vertical diffusion is parameterized within the planetary boundary layer as explained in section 2.1.5.

In **CLIO2**, the same equation as in the AGCM is resolved for the potential temperature θ and salinity S:

$$\frac{\partial \theta}{\partial t} + \left(\overrightarrow{u} \cdot \overrightarrow{\nabla_h}\right)\theta + w\frac{\partial \theta}{\partial z} = D_\theta + F_\theta^{surf} + F_\theta^{vol}$$

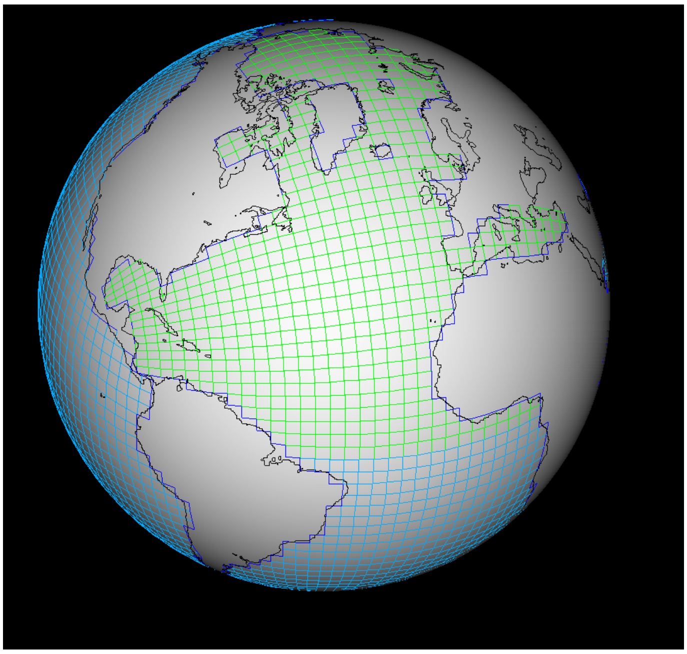

Figure 2.1: Grid used in CLIO2.

$$\frac{\partial S}{\partial t} + \left(\overrightarrow{u} \cdot \overrightarrow{\nabla_h}\right) S + w\frac{\partial S}{\partial z} = D_S + F_S^{surf}.$$

No volume source are taken into account for salinity but the solar radiation is assumed to penetrate below the sea surface (see section 2.1.3). D_θ and D_S account for the effects of small-scale processes not explicitly represented by the model. They have been classically parameterized by a diffusion term (*Goosse* [1998]):

$$D_\varepsilon = \kappa_{\varepsilon h}\overrightarrow{\nabla_h}^2 \varepsilon + \frac{\partial}{\partial z}\left(\kappa_{\varepsilon z}\frac{\partial \varepsilon}{\partial z}\right),$$

where the subscript ε stands either for θ or S.

2.1.1.4 Equation of state

The equation of state describes the dependence of density to other physical fields. LMD5 assumes that the air is in first approximation an ideal gas. Its equation of state thus relates density to pressure and temperature. In CLIO2, the equation of state follows *Eckart* [1958]. The seawater density is controlled by its potential temperature, salinity, and depth as described in *Campin* [1997]. The snow and ice densities are constant in the sea-ice model ($\rho_s = 330\,\mathrm{kg\,m^{-3}}$ and $\rho_i = 900\,\mathrm{kg\,m^{-3}}$).

2.1.2 Grids and numerical methods

In **CLIO2**, the numerical resolution of the equations governing the oceanic evolution is based on a finite-volume technique. The variables are staggered following a B-grid in the classification of Arakawa (*Mesinger and Arakawa* [1976]). The most natural way to discretize equations on the Earth is to use spherical coordinates. However, in this kind of grid, there is a singularity at the poles. This does not cause any trouble at the South Pole since it is located well inside the continent, but it is not the case at the North Pole. Consequently, the CLIO model uses two spherical subgrids (figure 2.1), which are described in detail in *Deleersnijder et al.* [1993] and *Campin* [1997]. The first one is based on classical longitude-latitude coordinates. It covers the Southern Ocean, the Pacific Ocean, the Indian Ocean, and the South Atlantic Ocean. The second subgrid covers the North Atlantic Ocean and the Arctic Ocean. It has its poles located at the equator, one in the Pacific Ocean (111°W) and one in the Indian Ocean (69°E). The two subgrids are connected in the Atlantic Ocean along the equator. A parameterization is used to simulate the water and ice flows through the Bering Strait (*Goosse et al.* [1997]). In both subgrids, the grid side is 3° in latitude by 3° in longitude. The vertical discretization follows the simple so-called "z-coordinate" (*Campin* [1997]). This means that the depth of each level is fixed as well as the location of the interface between levels. The bottom of the ocean is considered as a succession of steps. The vertical resolution is fine close to the surface and coarser in the deep ocean. There are 20 levels ranging from 10 m at surface to a maximum of 750 m near the bottom. The depth and thickness of the vertical layers are given in *Goosse* [1998]. The discretization of the time derivates in the governing equations uses a time step of 1 day for scalars. This choice ensures a good representation of the oceanic evolution and is long enough to limit the CPU[1]-time consumption. For the dynamical variables, two time steps are used. The barotropic part[2] of the oceanic circulation is integrated with a small time step of 5 min but it is a two-dimensional mode. The CPU-time consumption therefore remains reasonable. The three-dimensional baroclinic part[3] is solved using a much longer time step (3 hours). More details about this method can be found in *Campin* [1997]. This leads to good results as the fastest waves that the model must resolve (the surface gravity waves) influence the barotropic dynamics of the ocean. The physical parameterizations (see section 2.1.3) are called once a day.

The **sea-ice component** uses the same horizontal grid as the oceanic model. From a dynamic point of view, sea ice is seen as a two-dimensional continuum. In the thermodynamic parameterizations (see section 2.1.4), the sea-ice pack is divided into 3-layers. Sea ice is considered as an homogeneous slab divided into two layers of equal thickness, on which a snow layer can be present. The discretization of the governing equations follows the finite difference approach (see *Morales Maqueda* [1995]). The time step used for the discretisation of the time derivates is 1 day and the thermodynamic parameterizations (see section 2.1.4) are called once a day.

The spatial discretization of the equations governing the **atmosphere** is resolved using the classical spherical coordinates (longitude and latitude) in LMD5. They are 64 points equally spaced in longitude and 50 points equally spaced in sine of latitude (figure 2.2). This grid has a fine resolution in latitude at the equator and a coarse resolution near the poles. The advantage of this kind of grid is that each grid cell has the same area. This grid has two singularities at the poles. To avoid numerical problems, a filter is used. The vertical discretisation is based on the sigma-coordinate (see above). Our version of the LMD's

[1] Central Processing Unit
[2] depth-integrated part
[3] depth-dependent part

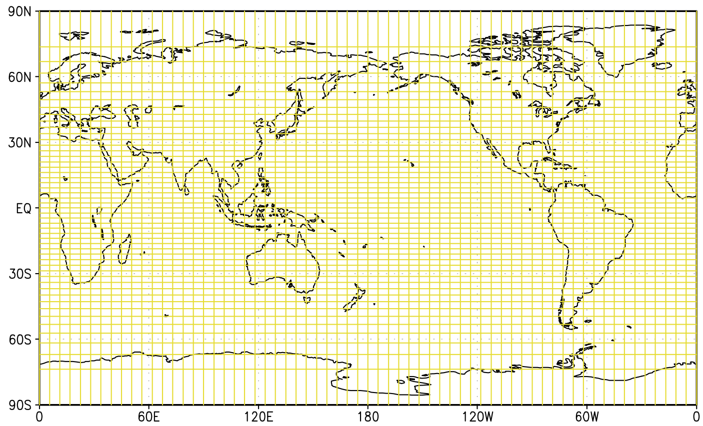

Figure 2.2: Grid used in our version of LMD5.

model has 15 vertical levels with a finer resolution near the surface. The numerical methods used in the model are described in Sadourny's papers (*Sadourny* [1975a]; *Sadourny* [1975b]; *Sadourny* [1980]). They are based on finite differences and a C-grid in the classification of *Arakawa and Lamb* [1977]. The dynamic time step to solve the time derivatives in the governing equations is 6 min. The physical parameterizations are called every 30 min, except the CPU-time consuming radiative scheme which is called every 6 hours. The water vapour advection scheme has been modified according to *Codron and Sadourny* [2002] in order to avoid unrealistic simulation of clouds and precipitation over high orography. The classical upstream scheme has been replaced by a new scheme that takes into account the local temperature. Indeed, the advected water vapour is constrained by saturation values.

2.1.3 Oceanic parameterizations

2.1.3.1 Surface layer heat budget

The surface heat budget (figure 2.3) takes into account the shortwave, longwave, sensible and latent heat fluxes (respectively F_{sw}, F_{lw}, F_{sens}, and F_{lat}) between the ocean and the atmosphere. A latent heat flux is associated to the evaporation at the ocean surface, another is due to the melting of snowfall falling into the ocean. The latent, sensible, and infrared heat fluxes can be safely considered as surface fluxes, all the exchanges taking place in the top centimeter or so. However, that is not at all true for the solar radiation, a significant amount of heat being absorbed in the ocean at depth. To take this effect into account, it is assumed that the extinction of solar radiation follows the parameterization of *Paulson and Simpson* [1977]: $F_{sw}(z) = F_{sw}i(z)$ where i is an extinction coefficient and z is the depth. The same procedure is applied for the solar flux which is coming to the ocean through the ice ($F_{sw}^{(to)}$). The surface heat budget at the top of the leads is $B_l = iF_{sw} - F_{lw} - F_{sens} - F_{lat}$.

The surface heat budget at the top of the open water is not the only contribution to the evolution of the upper oceanic layer temperature. A part of the solar flux F_{sw}^i goes into the subsurface oceanic layers. When sea ice is present in the grid cell, the heat flux at the sea-ice base F_w, the latent heat released by lateral accretion of sea ice or by snow ice

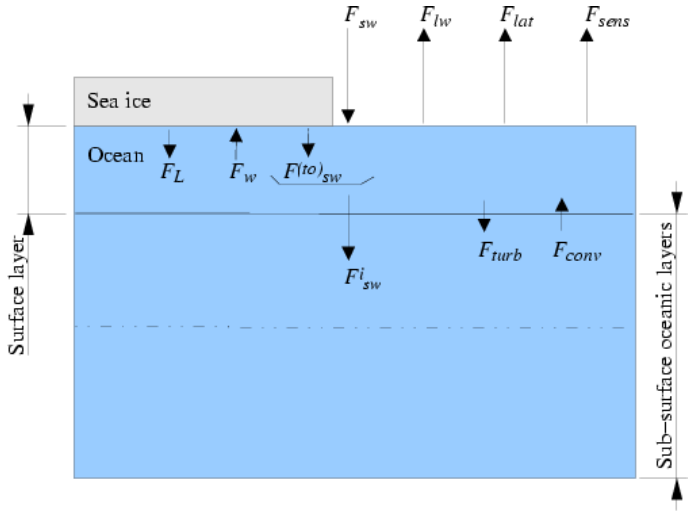

Figure 2.3: Heat budget of the oceanic surface layer. The symbols are explained in the text.

formation F_L, and the solar heat flux through the ice $F_{sw}^{(to)}$ also influence the sea-surface temperature. At the interface between the first and second oceanic layers, convection and turbulence in the oceanic column implies heat exchanges (see below). Moreover, it should of course been kept in mind that advection has an impact on the temperature field.

At the surface, the incoming solar radiation is partly reflected by the surface according to the *albedo*. Over the ocean, a simplified version of the parameterization of *Payne* [1972] is used. The sea-surface albedo α_{su} is equal to 0.06 for totally overcast conditions and for clear sky conditions: $\alpha_{su} = \frac{0.05}{1.1\cos^{1.4}(\mu)+0.15}$. When the sky is partly overcast, a linear interpolation is performed between these two extreme values, function of the cloud fraction.

2.1.3.2 Surface layer mass budget

In this version of the model, any freshwater flux is modeled as an equivalent salt flux (see *Goosse* [1998]). The surface freshwater budget at the top of open water gathers rainfall (rainfall falling on sea ice is assumed to be transfered directly to the ocean), snowfall over the leads, evaporation and runoff. The sea-ice thermodynamics induces other salt/water fluxes: the melting of snow, the net accretion/ablation of ice, the formation of snow ice (freezing of infiltrated water and modification of the snow salinity) as described in *Goosse* [1998]. All theses processes are described later in section 2.1.4.

2.1.3.3 Vertical mixing

The vertical mixing parameterization takes into account small-scale mixing processes (10 to 100 m). This small-scale *turbulence* is mainly located *in the* ***surface mixed layer*** (the upper hundred meters or so). It induces mixing in all directions (isotropic turbulence). Nevertheless, the oceanic grid cells are highly anisotropic: about 300 km horizontally and about 10 m vertically in the upper layers. Consequently, the mixing is mainly vertical.

The simplest way to parameterize vertical mixing is to use diffusion assuming that the diffusivity and viscosity depend on some local variables (see for example *Pacanowski and Philander* [1981]). A more sophisticated description of vertical mixing has been introduced in CLIO2. It follows *Kantha and Clayson* [1994]'s version of Mellor and Yamada's level 2.5 model (*Mellor and Yamada* [1982]). More details about this vertical turbulence scheme can be found in *Goosse* [1998], who studied the impacts of this parameterization on the model results (see also *Goosse et al.* [1999]).

Furthermore, a ***background diffusivity*** is imposed, following a vertical profile described in *Campin* [1997]. The background viscosity is constant below 150 m, and increases upwards.

The grid resolution and the approximations used to simplify the equations (mainly the hydrostatic approximation) do not allow to have and explicit description of the strong ***convection***. Indeed, convection occurs in region of horizontal length scale of a few kilometers and it involves locally intense vertical velocities. This physical process is therefore not directly resolved by the model dynamics. Furthermore, Mellor-Yamada's model is not designed to work properly in these circumstances. Consequently, a new parameterization is introduced in CLIO2. It consists of an increase of the vertical diffusivity whenever the vertical density profile is unstable (*Goosse* [1998]). This induces intense vertical mixing.

2.1.3.4 Downsloping currents

Surface water gets denser around Antarctica because of strong ice production and cold atmospheric conditions. This dense water forms on the Antarctic shelf and tends to sink along the slope of the sea floor at the shelf break. AABW (Antarctic Bottom Water) flows this way to great depth. This mechanism differs strongly from convection as the mixing with surrounding water is not very important. Furthermore, the coarse model resolution and the z-coordinate used lead to a topography looking like a staircase with steps of hundreds of kilometers or so wide and from about a ten or a thousand meters high. This kind of configuration is not appropriate to simulate a current flowing along the slope. Consequently, the downsloping currents have to be parameterized in CLIO2. The approach of *Campin and Goosse* [1999] has been followed. The flow itself is not represented, only its impact on water properties is simulated. This approach is more relevant to coarse resolution models.

2.1.3.5 Horizontal meso-scale eddies

Quasi-horizontal eddies of a hundred of kilometers wide or so imply mixing. This turbulence is not isotropic. The mixing is more intense along the isopycnal surfaces[4] than in a diapycnal[5] direction. The effects of these eddies on the mean field are classically parameterized by a diffusion term implying horizontal and vertical diffusivity. This is the simplest way to deal with diffusion as the model is written in z-coordinate. However, it would be more appropriate to separate the isopycnal diffusion and the diapycnal diffusion. These improvements have been included in another version of the model.

[4] Isopycnals are surfaces of constant density.
[5] perpendicular to the isopycnals.

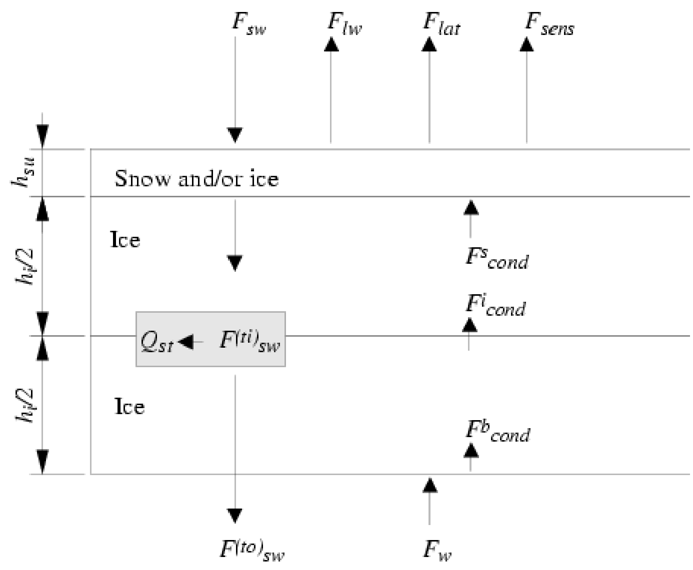

Figure 2.4: Heat budget of the ice pack. The symbols are explained in the text.

2.1.4 Sea-ice parameterizations

The floes within the ice pack are separated by zones of open water: leads and polynyas. These areas of open water are very important, even if they cover only a small fraction of the surface. They allow direct exchanges between the atmosphere and ocean and thus much stronger fluxes than when ice is present (see chapter 1). This fraction of open water is represented in the model by the introduction of the ice concentration. This variable A is the percentage of each cell which is covered by ice. The thermodynamics is resolved for the ice pack (these processes are gathered hereafter under the title vertical growth and decay of the ice), and for the leads (these processes are called lateral growth and decay of the ice). A complete description of the parameterizations can be found in *Fichefet and Morales Maqueda* [1997].

2.1.4.1 Vertical growth and decay

The parameterization of the vertical growth and decay of sea ice is an improved version of the 3-layer model of *Semtner* [1976]. Sea ice is considered as an homogeneous slab divided into two layers of equal thickness, on which a snow layer can be present. The temperature T_c and the thickness h_c of these three layers are computed (the subscript c stands either for the ice i or snow s). On the Earth, the sea-ice thickness is of course not uniform over areas as big as the model grid cells. A first attempt is made in CLIO2 to implicitly include a range of thicknesses. It is assumed that the snow and ice thicknesses are uniformly distributed between zero and twice their mean value over the ice-covered part of the grid cell. This influences the conductive flux through sea ice.

Figure 2.4 illustrates the heat budget of the ice pack. It provides a visual idea of most heat fluxes.

At the *surface* of the snow-ice system, the ***heat budget*** of a thin layer of thickness h_{su}

is considered:

$$h_{su}(\rho c_p)_{su}\frac{\partial T_{su}}{\partial t} - \left(\frac{\partial h_{su}}{\partial t}\right) L_{su} = (1-i_0)F_{sw} - F_{lw} - F_{sens} - F_{lat} + F^s_{cond}.$$

The subscript su stands either for ice or for snow depending on what is present at the top of the snow-ice system. F_{sw}, F_{lw}, F_{sens}, F_{lat}, and F^s_{cond} are the shortwave, longwave, sensible, latent and conductive heat fluxes, respectively. $(\rho c_p)_{su}$ is the density time the specific heat of the surface layer. i_0 is the fraction of solar radiation which is not absorbed in the thin surface layer and penetrates inside the ice cover (see *Fichefet and Morales Maqueda* [1997]). The left hand part of this equation indicates that the net heat flux change the surface temperature. Furthermore, if the heat balance requires the surface temperature to be above the melting point, T_{su} is held at this point and the excess of energy is used to melt snow or ice and consequently to change the ice or snow thickness. L_{su} is the volumetric latent heat of fusion of snow or ice.

F_{sw} is the absorbed fraction of the incoming solar radiation. It depends of the surface *albedo*. The albedo for snow and ice is a function of the surface characteristics (snow or not, melting or not, ice and snow thicknesses) as proposed by *Shine and Handerson-Sellers* [1985]. Furthermore, as suggested by *Grenfell and Perovich* [1985], the albedo is increased (in our version by 0.04) under overcast conditions to take into account the selective absorption of shortwave radiation by clouds. The dry or melting snow, bare puddled or frozen ice albedos are empirical estimates. They have been modified in this version to improve the simulated Arctic sea ice. Their respective values are 0.72, 0.55, 0.48 and 0.64. An interpolation between the melting and frozen values has also been included for surface temperature between the freezing point and this point minus 1 K.

Inside the snow-ice system, the evolution of temperature is governed by the one-dimensional *heat diffusion equation*

$$(\rho c_p)_c\frac{\partial T_c}{\partial t} = Gk_c\frac{\partial^2 T_c}{\partial z^2},$$

where k_c is the thermal conductivity. T_c is the temperature. G is a correction factor which represents the effects of the subgrid-scale snow and ice thickness distributions on the conductive heat flux (see *Fichefet and Morales Maqueda* [1997] for more details). Subsequently, the conductive heat flux is $F_{cond} = -Gk_c\frac{\partial T_c}{\partial z}$. The sea-ice conductivity is taken equal to $k_i = 2.0344\mathrm{Wm}^{-1}\mathrm{K}^{-1}$, and the snow conductivity has been reduced to $k_s = 0.21\mathrm{Wm}^{-1}\mathrm{K}^{-1}$ compared to the standard value $k_s = 0.3098\ \mathrm{Wm}^{-1}\mathrm{K}^{-1}$. This modification has improved the model results in the Arctic Ocean. This change has been suggested by a similar study involving the Antarctic sea ice (*Fichefet et al.* [2000]).

The part of the shortwave radiation absorbed inside the ice does not change the ice temperature but is rather stored in a heat reservoir Q_{st} that represents internal meltwater in *brine pockets*. Assuming an exponential absorption of shortwave radiation within the ice, the solar heat flux absorbed inside the ice is $F^{(ti)}_{sw} = i_0 F_{sw}[1-e^{-1.5(h_i-h_{su})}]$. Q_{st} evolves according to

$$\frac{\partial Q_{st}}{\partial t} = F^{(ti)}_{sw} - F_{lbp},$$

where F_{lbp} is the heat flux necessary to prevent the upper ice layer from cooling below its melting point. The solar energy is stored in spring in this reservoir. This latent heat is released in autumn through the refreezing of the brine pockets. The seasonal cycle of the ice temperature is thus shifted from the insulation one: the spring and summer shortwave energy is stored instead of implying a warming and the refreezing of ice pockets avoids a rapid cooling of the ice pack in autumn. The shortwave radiation which is not trapped in the ice pack is transmitted to the underlying ocean $F_{sw}^{(to)} = i_0 F_{sw} e^{-1.5(h_i - h_{su})}$.

When the load of snow is large enough to depress the lower boundary of the snow layer under the water level, seawater is assumed to infiltrate the submerged snow and to freeze there, forming *snow ice*. The balance between the snow ice pack weight and the Archimedes buoyant force determines the submerged part of the snow ice pack and thus the variation of the snow and ice heights (see *Fichefet and Morales Maqueda* [1997] for details). The latent heat and salt released in the freezing of seawater are discharged into the ocean.

At the *bottom* of the ice slab, the ice temperature is assumed to remain to the seawater freezing point. Consequently, any imbalance between the conductive heat flux within the ice F_{cond}^{b} and the heat flux from the ocean to the ice F_w is compensated by an accretion or ablation of ice:

$$\frac{\partial h_i}{\partial t} = \frac{F_{cond}^{(to)} - F_w}{L_i}$$

where L_i is the volumetric heat of fusion of ice. $F_w = \rho_0 c_{pw} c_h u_* (T_{ml} - T_f)$, i.e. the oceanic heat flux depends on the difference between the oceanic mixed layer T_{ml} (taken as the upper OGCM layer) temperature and the seawater freezing temperature T_f. u_* is the friction velocity linked to the ice-ocean stress (see *Goosse* [1998] for more details). $c_h = 0.006$ is an empirical constant.

2.1.4.2 Lateral growth and decay

The thermodynamic variations of the ice concentration A are function of the heat budget B_l of the leads that cover a fraction $1 - A$ of the grid cell. B_l is computed in the same way as the heat flux towards the ocean (see section 2.1.3.1).

If the lead heat budget is negative and would bring the sea-surface temperature (SST) below the seawater freezing point, the SST remains fixed to this point and new ice, at the same temperature, is created according to the equation:

$$\frac{\partial A}{\partial t} = -\Phi(A)\frac{(1 - A)B_l}{L_i h_0}.$$

The ice formed in the lead has a thickness h_0 but only a fraction $\Phi(A)$ of the ice formed contributes to the increase of the ice concentration. The remaining part is rather assumed to lead to an increase in the thickness of the pre-existing ice (*Fichefet and Morales Maqueda* [1997]). Whenever *lateral accretion* of ice occurs, the thickness of newly formed ice is averaged which that of pre-existing ice to obtain a single value and snow is distributed over the new ice-covered area. The internal ice temperatures are modified accordingly.

The lead heat budget does not influence the oceanic surface layer temperature. If it is positive, the entire heat gain in the leads contributes to the basal melting. A vertical decay of the ice pack is thus assumed. Nevertheless, taking into account the uniform distribution in thickness between 0 and $2h_i$ (see above) over the ice-covered fraction of the grid cell,

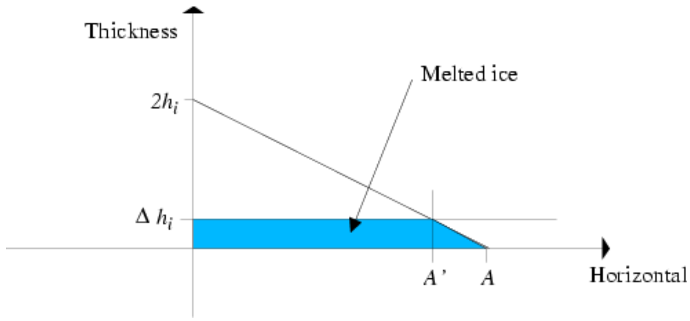

Figure 2.5: Concomitant reduction in ice concentration and thickness assuming a uniform distribution in thickness between 0 and $2h_i$.

vertical melting necessarily implies a *concomitant reduction in ice concentration* (figure 2.5) *and in the ice thickness* to conserve the ice volume :

$$\frac{\partial A}{\partial t} = -\frac{A}{2h_i}\Gamma\left\{-\left(\frac{\partial h_i}{\partial t}\right)\right\},$$

where Γ is the Heaviside unit function[6] (*Fichefet and Morales Maqueda* [1997]). All the variations of the ice thickness are taken into account in $\frac{\partial h_i}{\partial t}$: ablation or accretion at the surface or at the bottom, and snow ice formation. When the ice concentration decreases, the snow present at the surface is piled up onto the remaining ice.

Exchange of momentum between sea ice and the underlying ocean

The stress at the interface between the ocean and sea ice is function of a drag coefficient and the square of the difference between the ice velocity and the oceanic surface layer velocity (assumed to be the oceanic upper layer velocity). Details of this parameterization are discussed in *Goosse* [1998].

2.1.5 Atmospheric parameterizations

The hydrological cycle deals with water phase transformation. The atmosphere contains humidity that is partly vapour, liquid, or water in suspension (as cloud droplets or ice crystals), or precipitating liquid or solid water (as rain or snow). The presence of humidity in the atmosphere implies interactions with ocean, sea ice, and soil and vegetation: **evaporation**, **precipitation**, evapotranspiration, **soil hydrology**, ...

When water condensates in the atmosphere, **clouds** appear. They have a significant impact on **radiation,** which is the basic source of energy for the Earth system. In order to simulate climate evolution, the model should reproduce correctly the amount and properties of clouds. Small particles in the atmosphere called **aerosols** also influence the radiative budget of the Earth system.

Near the surface other energy fluxes are involved: latent and sensible heat fluxes. They result from **turbulence** near the Earth's surface and characterize the interactions between the climate system components.

[6] The Heaviside unit function is defined as follow: $\Gamma(x) = 1$ if $x \geq 0$, and $\Gamma(x) = 0$ if $x < 0$.

All these physical processes have been described in chapter 1. They involve smaller length scales than LMD5 grid cell size. Subsequently, they can not be explicitly resolved by the model. They must be parameterized, i.e., these processes have to be expressed in term of large-scale variables. The main parameterizations of LMD5 are briefly described hereafter.

2.1.5.1 Cloud formation

Clouds form in three cases. Firstly, when the atmospheric column is instable over a wide vertical extend, deep convection occurs. It leads to *cumulus clouds* which penetrate deeply in the troposphere. Deep convection is mainly present in the tropics. Secondly, shallow convection is also associated with convective motions, but is constrained mainly inside the boundary layer (the lower 5 levels in our AGCM). Finally, a layer may reach saturation independently to vertical motions. In that case, *stratiform clouds* appear.

To determine if convective cloud should form, the model compares the vertical temperature gradient to critical lapse rates. In an unsaturated atmospheric column, the lapse rate is $\Gamma_d = \frac{g}{c_p}$ where g and c_p are respectively the gravity constant and the air heat capacity[7]. According to *Manabe and Strickler* [1964], the model modifies the temperature profile to avoid vertical temperature gradients greater than this dry critical lapse rate. In a super-saturated atmospheric column, one should take into account heat released by condensation. The critical lapse rate[8] becomes $\Gamma_m = \frac{g}{c_p}\left(1 + \frac{Lq_s}{RT}\right)\left(1 + \frac{L}{c_P}\frac{\partial q_s}{\partial T}\right)^{-1}$ where L is the latent heat of vaporization, q_s represents the specific humidity at saturation, R is the gas constant, and T is temperature. This threshold is used for moist convection. Two moist convection cases are parameterized in the LMD's model (*Li* [1998]).

1. If the air is super-saturated and unstable, i.e., $q > q_s$ and $\frac{\partial T}{\partial z} < -\Gamma_m$, a moist convective adjustment after *Manabe and Strickler* [1964] is carried out. The temperature profile is adjusted to the moist adiabatic lapse rate $\frac{\partial T'}{\partial z} = -\Gamma_m$ and the specific humidity is set to the saturated profile for the adjusted temperature T', i.e., $q' = q_s(T', p)$, with the total moist static energy in the column being held constant

$$\sum_{l=base}^{l=top} \{[c_p[T'(l) - T(l)] + L[q'(l) - q(l)]]d\sigma_l\} = 0,$$

   to ensure energy conservation. $d\sigma_l$ is the layer thickness. The excess of moisture contributes to the liquid water content (LWC) and the fractional area of the convective cloud is set equal to 1.

2. Convection can also occur in unsaturated air if the temperature lapse rate is conditionally unstable, $\frac{\partial T}{\partial z} < -\Gamma_m$. According to *Kuo* [1965], the formation of a cumulus cloud depends on the moisture convergence into the cloud. The height of the cumulus cloud is given by the highest level for which the moist static energy

[7]This critical lapse rate comes from the conservation of dry static energy $s = c_pT + gz$ during an adiabatic ascent without condensation (*Holton* [1992]).

[8]This critical lapse rate comes from the conservation of moist static energy $h = c_pT + gz + Lq_s$ during an adiabatic ascent when saturation is reached (*Holton* [1992]).

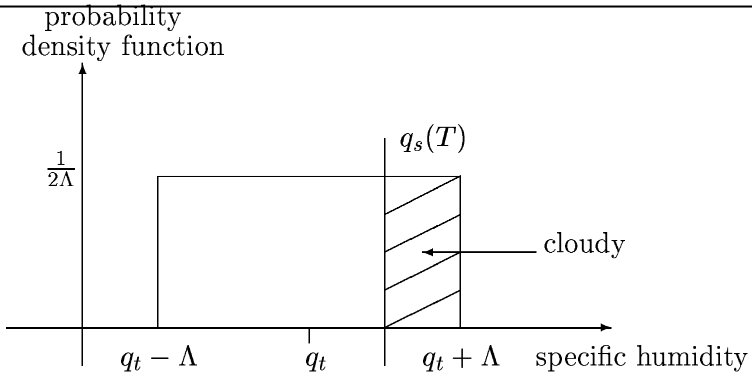

Figure 2.6: This sketch shows the probability density function for any specific humidity. This probability distribution is uniform between $q_t - \Lambda$ and $q_t + \Lambda$.

($h = c_pT + gz + Lq$) is less than that at the cloud base. It means that the air parcel from the cloud base has enough energy to move up to that level. All the humidity entering any cloudy layer since the last call of the convective scheme is pumped into the cloud. It determines the moisture convergence Δ. It contributes to reach cloud temperature and humidity profiles, which are those of a moist adiabatic atmosphere (i.e., $h_{cloud}(l) = h_{base}$ and $q_{cloud}(l) = q_s(T_{cloud}, p)$). The amount of humidity needed to reach those over the whole grid box is:

$$\Delta_t = \sum_{l=base}^{l=top} \{[q_s(l) - q(l) + \frac{h(l) - h_{base}}{L}]d\sigma_l\},$$

where $d\sigma_l$ is the layer thickness. Therefore, the cloud fraction f is calculated as the ratio of the available humidity Δ and the "needed" humidity Δ_t. As a result of mixing, the environmental (grid-scale) temperature and humidity profiles evolve towards the moist adiabatic values in proportion to this fractional cloud area: $T'(l) = T(l) + f\delta T$ and $q'(l) = q(l) + f\delta q$. The excess of moisture contributes to the LWC.

Formation of stratiform clouds is handled by a stochastic approach (*LeTreut and Li* [1991]). An uniform probability distribution around the mean total humidity, q_t (liquid plus vapour), is assumed with a prescribed standard deviation 2Λ. The fraction of stratiform cloud in any layer is determined from the probability that the water amount q (liquid plus vapour) is above the saturation value q_s (figure 2.6).

Whenever saturation is reached, i.e., $q_s \in (q_t - \Lambda, q_t + \Lambda)$, the cloud fraction f is the dashed part on figure 2.6. Consequently, $f = \int_{q_s}^{q_t+\Lambda} \frac{1}{2\Lambda}\, dq = \frac{q_t+\Lambda-q_s}{2\Lambda}$ and the liquid water which arises by condensation is $LWC = \int_{q_s}^{q_t+\Lambda} \frac{1}{2\Lambda}\,(q - q_s)\; dq = \frac{(q_t+\Lambda-q_s)^2}{4\Lambda}$. The corresponding latent heat is released and changes the temperature. q_s being a non-linear function of temperature, it is necessary to iterate in order to adjust T' and q_s.

The Λ parameter is proportional to the humidity q_t: $\Lambda = \gamma q_t$. As explained by *Grenier* [1995], the representation of strato-cumulus clouds by the LMD's model is improved by decreasing the coefficient γ in the lowest layers of the atmosphere. Indeed, when the width of the humidity distribution is reduced, the transition between an uncloudy layer and a fully cloudy layer is more abrupt, i.e., the cloud fraction shifts rapidly from 0 to 1. Furthermore, the cloud liquid-water content then rapidly increases when a cloud is formed. Physically, it is consistent with large stratiform clouds where small fluctuation of the relative humidity are observed over a great area. The turbulence being more intense near the surface, it seems tenable to assume that the humidity distribution is more uniform in the lowest atmospheric layers. In our version of the model, the following values have been chosen: $\gamma = 0.3$ from the forth layer to the top of the atmosphere, $\gamma = 0.05$ in the lowest two layers, and in the third layer $\gamma = 0.3$ at high latitudes, and $\gamma = 0.05$ at mid- and low latitudes.

2.1.5.2 Precipitation

The processes involved in precipitation are different for warm (water) clouds and cold (ice) clouds.

In each grid box, warm clouds constitute a fraction x and cold clouds a fraction $1 - x$ of the total cloud cover. x is taken equal to 0 for temperatures below 253 K and 1 for temperatures above 263 K, and we assume that it varies linearly between these values at intermediate temperatures. These threshold temperature values have been chosen after some sensitivity experiments. The aim of these changes was to improve the surface radiative heat budget over the Southern Ocean. Indeed, as explained below later on, the cloud optical properties differ for warm and cold clouds.

For warm clouds, the precipitation rate is parameterized after *Sundqvist* [1981]: $P = \frac{l}{C_t}[1 - e^{-\left(\frac{l}{C_t}\right)^2}]$, where l is the prognostic cloud liquid mixing ratio, $C_t^{-1} = \frac{1}{5.5 \times 10^{-4}}$ s is a characteristic precipitation time scale, and C_l is a prescribed precipitation threshold value taken equal to $2 \times 10^{-4}\,\mathrm{kg\,kg^{-1}}$.

For cold clouds, the precipitation rate depends on the terminal velocity V according to *Heymsfield and Donner* [1990]. So, the liquid water falling out of a layer, whose depth is δz, is $P = l\frac{V}{\delta z} = \frac{l}{\delta z}\frac{3.29}{C}(\rho l)^{0.16}$ where $\frac{3.29}{C}$ is an empirical parameter. According to *Grenier* [1995], this parameter has been modified to keep more humidity in the tropical atmosphere. After some sensitivity experiment, the following value has been chosen: $C = 2$.

Evaporation of falling convective and large-scale precipitation is not explicitly modeled, but evaporation of small stratiform cloud droplets making up the LWC is simulated stochastically.

Precipitation falls as snow whenever the first level temperature is lower than 271.15 K, and snowfall is avoid whenever this temperature is higher than 273.15 K. Between these threshold values, the fraction of snowfall in the total precipitation changes linearly. This has been introduced in our version of the LMD's model to try to restrain snow ice formation in the Northern Hemisphere.

2.1.5.3 Evaporation

Evaporation over land is determined by the SECHIBA scheme (*Ducoudré et al.* [1993]) which is a vegetation scheme. For each continental grid box, eight coexisting land surface types are specified from aggregation of the data of *Matthews* [1983] and *Matthews* [1984] :

bare soil, tundra, grassland, grassland with shrub cover, grassland with tree cover, deciduous forest, evergreen forest, and rain forest. A fractional area of the grid box, as well as some prescribed canopy characteristics, are associated with each of these eight land surface types.

The evaporation flux is computed separately for each of the eight coexisting land surface types. The total evaporative flux from land is then computed as an area-weighted average of the individual fluxes. The total flux includes sublimation from snow, evaporation from bare soil and from moisture intercepted by the canopy of each vegetation class, and transpiration from the dry foliage of each class. Sublimation and evaporation from intercepted canopy moisture occur at the potential rate, while canopy transpiration and evaporation from bare soil depend on the surface relative humidity which is parameterized in terms of soil moisture. Evaporation from subcanopy soil is neglected. The surface moisture flux is computed by a bulk method and depends on the moisture gradient between the surface and the overlying air and on resistances of different kinds (aerodynamic, soil, architectural, and canopy) that vary according to surface type and/or the nature of the moisture flux (sublimation, evaporation, transpiration).

Furthermore, evaporation is calculated over ocean as a function of wind speed, and of the difference between the saturation specific humidity at the sea-surface temperature and the extrapolation of the atmospheric specific humidity towards the surface. The proportionality coefficient, called drag coefficient, is parameterized according to *Louis* [1979] (see *Grenier* [1995]).

2.1.5.4 Runoff and soil moisture

Soil hydrology is simulated using the land-surface scheme SECHIBA of *Ducoudré et al.* [1993].

The snow pack thickens according to snowfall and decreases when the surface temperature exceeds 0°C. Water resulting from the snow melting goes into the soil moisture reservoir. Rainfall (only liquid precipitation) contributes directly to the soil moisture and to evaporation.

The total depth of the soil column (corresponding to the vegetation root zone) is set equal to 1.0 m. Soil moisture is computed in two layers, the upper layer being the most reactive: when precipitation exceeds evapotranspiration, the upper layer fills first; when the reverse is true, it empties first. Runoff occurs whenever the soil column is completely saturated (water depth exceeding 0.15 m). The remaining prescribed parameters for bare soil are a constant evaporation resistance and an empirical constant used to compute surface relative humidity for calculation of evaporation.

The runoff water is instantaneously transfered to the ocean. LMD5 grid cells can cover ocean or land according to the oceanic mask determined by CLIO2. LMD5 grid cells which overlap partially or totally the oceanic surface release the runoff directly in the underlying CLIO2 grid cells. The land-only grid cells are gathered in drainage basins (figure 2.7) that bring water to a grid cell that overlies ocean. This represents in a much simpler way the flow of a river towards its mouth.

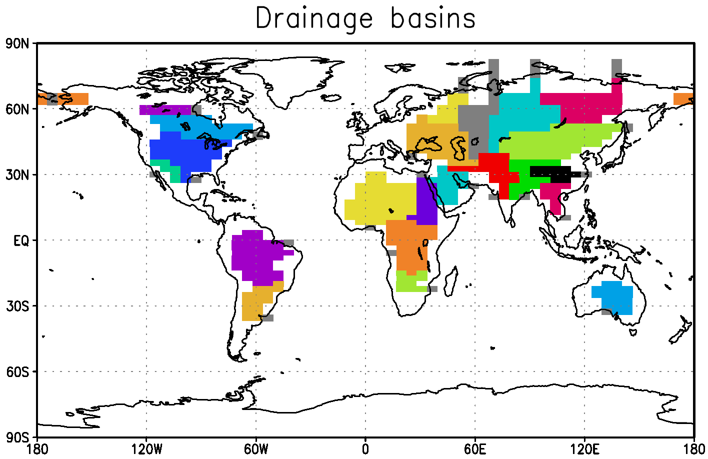

Figure 2.7: The largest 23 drainage basins defined in LMD5-CLIO2 and their mouth (in grey).

2.1.5.5 Radiation

The energy source for the Earth system is radiation coming from the Sun. Because of its temperature the sun emits in the visible wavelengths. After partial diffusion and reflection in the atmosphere, the solar energy reaches the surface where it is partly reflected and partly absorbed. **Shortwave radiation** is modeled after an updated scheme of *Fouquart and Bonnel* [1980]. The diurnal cycle of insulation is not resolved, and solar constant is fixed to 1368 $\mathrm{W m^{-2}}$.

According to Stefan's law, the warmed Earth radiates energy in the infrared. On the contrary to what happens to solar radiation, some gases in the atmosphere are active at those wavelengths: the greenhouse gases. They absorb (trap) infrared radiation coming from behind and they re-emit radiation at their own temperature which is lower than that of the surface. **Longwave radiation** is modeled in six spectral intervals between wavenumber 0 and $2.82 \times 10^{-5}\,\mathrm{m^{-1}}$ after the method of *Morcrette* [1990] and *Morcrette* [1991]. The version of this scheme allows to treat the effect of each greenhouse gas separately.

Clouds play an important role in the radiative transfer. They reflect solar radiation towards space and they trap infrared radiation coming from the surface. They thus have two opposite impacts : cooling in the shortwave and warming in the longwave. Their action depends on their altitude. Low clouds are more dense (contain more water) and therefore are more efficient to reflect solar radiation. High clouds are colder, and so they re-emit less radiation towards space.

The model takes into account these two effects. The shortwave radiation scheme contains a parameterization of scattering by clouds.

- The asymmetry factor is prescribed: $c_g = 0.865$ for the spectral range between 0.25 and 0.68 micron and $c_g = 0.910$ for the the spectral range between 0.68 and 4.00 microns.

- The optical depth τ is a function of the cloud liquid water content l and the effective radius of cloud droplets r_e. In fact, $\tau = \frac{3}{2}\frac{W}{r_e}$ where r_e is prescribed as $12 \times 10^{-6}\,\mathrm{m}$

for warm clouds and as 40×10^{-6} m for cold clouds; these values have been chosen after some sensitivity experiments. $W = \int_{base}^{top} \frac{l}{\rho_l} dz$ is the integrated water path, *base* and *top* represent respectively the levels for base and top of the cloud, ρ_l is the liquid water density. Consequently, clouds containing a great amount of liquid water are optically thicker than clouds containing less liquid water. Furthermore, low clouds with smaller droplets are more efficient to scatter solar radiation. The optical depth is used to determined the single-scattering albedo, $\omega = 0.9999 - 5 \times 10^{-4} \exp\left(\frac{\tau}{2}\right)$.

In the longwave domain, clouds are treated as grey bodies. The droplet absorption is modeled through an emissivity $\epsilon = 1 - \exp(-k_a W)$ which is a function of the cloud liquid-water path. The absorption coefficient k_a is different for warm and cold clouds: $130\,\mathrm{m}^2\,\mathrm{kg}^{-1}$ and $50\,\mathrm{m}^2\,\mathrm{kg}^{-1}$, respectively.

For purpose of the radiation calculations, all clouds are assumed to overlap horizontally along the vertical. Three kinds of overlapping are available in the model (figure 2.8). Let's assume you are going up from the surface to the top of the atmosphere. The maximum overlapping (used in the previous version of the model) assumes that the cloud layers are nicely piled up over each other. For the random overlapping, the probability that the cloud layer overlaps the previous one is equal to the probability that the cloud layer is not over the previous one. Thirdly, the max-random overlapping uses the maximum overlapping inside a cloud and the random overlapping to form a new cloud if the cloudiness decreases and then increases again. After some sensitivity experiments, the max-random overlapping, which also seems more physical, has been chosen. It has produced an overall decrease in cloudiness. The reduction of low-level stratiform clouds at mid-latitudes weakens the greenhouse effect there, which leads to sea-surface temperatures that are in better agreement with observations in those areas. On the contrary, as convective tropical clouds are well stacked, the simulated net shortwave radiation at the surface is degraded with the max-random overlapping.

Over the land free of snow and ice, the **surface albedo** derives from the monthly data of *Dorman and Sellers* [1989], α_{clim}. The albedo of snow-covered surfaces is computed following *Chalita and LeTreut* [1994] as a function of the fractional area of snow cover, the snow age, the vegetation type, and the spectral range:

$$\alpha = \sum_{n=1}^{n=8} veg_n \, \beta \, as_n + (1-\beta)\alpha_{clim}$$

where veg_n is the fractional area covered by each land surface type (eight vegetation types) and β is the snow fraction. as_n is an albedo function of the snow age *age* and of the vegetation covered:

$$as_n = a_n + b_n \exp\left(\frac{-age}{t_c}\right)$$

where a_n, b_n are prescribed parameters, $t_c = 5$ is a critical value. Any snowfall implies a reduction of the snow age. This decrease is an exponential function of the intensity of the snowfall.

The parameterization of the direct effect of **sulphate aerosols** developed by *Mitchell et al.* [1995] has also been introduced into the AGCM and thoroughly tested. In this formulation the scattering of solar radiation by sulphate aerosols is crudely represented by

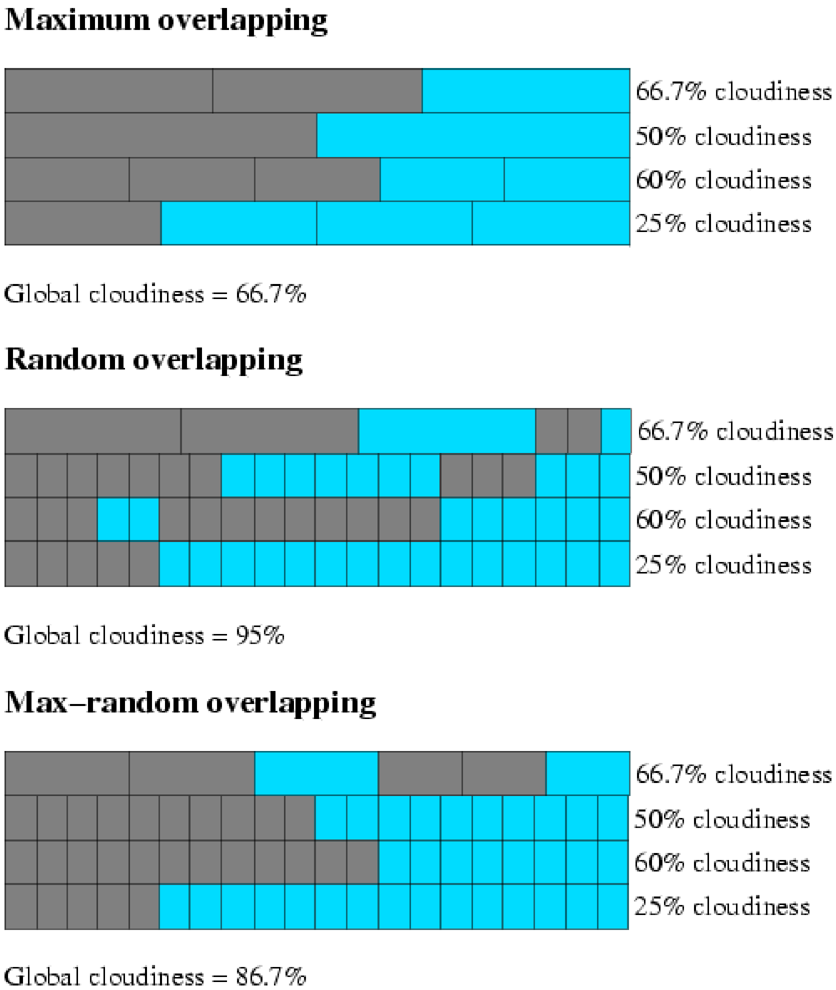

Figure 2.8: Horizontal cloud overlapping along the vertical. These figures show the cloud repartition in four consecutive layers in the atmosphere. The x-axis is the horizontal extent, the y-axis is the vertical. The grey boxes are cloudy, the blue boxes are clear sky. The maximum overlapping assumes that the cloud layers nicely pile up over each other. The random overlapping assumes that having a cloudy box over a cloudy box or a cloudy box over a clear sky box share the same probability. The max-random overlapping makes the same assumption than the maximum overlapping inside a cloud but, when the cloudiness decreases and increases again, a new cloud is formed and the random overlapping is used.

an increase in surface albedo. The effective increase in surface albedo due to scattering by aerosols is approximated by $\beta\delta\,(1-\alpha)^2\sec(\theta_0)$ where θ_0 is the solar zenith angle, α is the surface albedo, and $\delta = aB_{SO_4}$ is the optical thickness of the aerosol layer. B_{SO_4} is the aerosol loading (gm^{-2}) used as input. According to *Mitchell et al.* [1995], we use $\beta = 0.29$ and $\alpha = 5\ \mathrm{m^2g^{-1}}$. This modification is applied only in the clear-sky part of the grid cell.

2.1.5.6 Surface planetary boundary layer

The model planetary boundary layer (PBL) consists of the first 5 levels above the surface. At the sixth level, the vertical turbulent eddy fluxes of momentum, heat, and moisture are assumed to vanish.

Second-order vertical diffusion of momentum, heat, and moisture is applied only within the PBL (*Sadourny and Laval* [1984]). The diffusion coefficient depends on the turbulent kinetic energy (TKE) and on the mixing length (which decreases up to the prescribed PBL top) estimated following *Smagorinsky et al.* [1965]. Estimation of TKE involves calculation of a counter-gradient term after *Deardorff* [1966] and comparison of the bulk Richardson number with a critical value. More details can be found in *Grenier* [1995]. Following his work, the residual turbulent kinetic energy in a stable PBL is fixed to $10^{-10}\ \mathrm{m^2s^{-2}}$. This parameter has been reduced compared to previous versions of the LMD's model to keep more humidity in the PBL in order to improve the representation of strato-cumulus clouds.

At the surface, the turbulent fluxes are computed according to bulk aerodynamic formulas. The latent heat flux associated with evaporation is a function of the humidity gradient as already explained above. Similarly, the sensible heat flux depends on the temperature gradient between the surface and the overlying air (extrapolation from the first two atmospheric levels), on the surface wind velocity, and on a drag coefficient (determined as in *Louis* [1979]). More details can be found in *Grenier* [1995]. Finally, the surface wind stress is function of the surface wind and the surface roughness.

In order to account for the large difference in the turbulent heat fluxes over sea ice and leads or polynyas at high latitudes and to ensure conservation of heat and freshwater while transferring fluxes between the LMD5 grid to the CLIO2 grid, each surface grid box is divided into appropriate fractions of land, ocean, and eventually sea ice. The surface latent and sensible fluxes are computed separately (*Grenier* [1995]) over each surface type.

2.1.5.7 Gravity-wave drag

The formulation of gravity-wave drag closely follows the linear model described by *Boer et al.* [1984]. It accounts for the effect of the subgrid-scale orography. The drag at any level is proportional to the vertical divergence of the wave momentum stress This stress is formulated as the product of a constant aspect ratio, the local Brunt-Vaïsala frequency, a launching height determined from the orographic variance over the grid box, the local wind velocity, and its projection on the wind vector at the lowest model level. The layer where gravity-wave breakdown occurs (due to convective instability) is determined from the local Froude number. In this critical layer, the wave stress decreases quadratically to zero as a function of height.

2.1.6 Boundary conditions, and coupling between the AOGCM components.

The Earth's surface is the interface between the atmosphere above and the ocean, sea ice, or land below. Many interactions take place at this interface. The atmosphere needs the surface characteristics like the vegetation types, the albedo, the roughness length, the soil humidity, etc. to compute the surface water, heat, and momentum fluxes. Conversely, the ocean needs the surface fluxes to determine its temperature and its salinity. Sea ice uses the same atmospheric information to compute its thermodynamic and dynamic evolution. Over land, the surface heat and water budgets are also computed to determine the surface temperature and humidity.

The atmosphere and the continental surface are together in LMD5. Thus, the interactions are taken into account inside the model. The albedo, soil humidity, etc. are available to the atmospheric routines and conversely, the surface routines have access to the surface fluxes to compute the water and heat budgets.

Similarly, CLIO2 contains an oceanic component and an sea-ice component. The appropriate informations are shared by the two components.

On the contrary, specific methods have to been applied to transfer data between LMD5 and CLIO2. The first step is to identify the atmospheric and oceanic or sea-ice needs at their interface and to determine which model is best suited to determine these quantities.

The surface turbulent fluxes are required by the ocean and sea-ice components to determine their thermodynamic and dynamic evolution. If the surface temperature and characteristics are provided to the atmosphere, LMD5 is able to determine these fluxes according to the whole atmospheric boundary layer evolution. Taking into account the parameterizations in our models, this seems to be the best approach. Other modeling teams have made other choices. For example, the atmosphere and ocean model can provide a third model with their characteristics and this additional model computes the surface fluxes and gives them back to the atmosphere and ocean models. This flux coupler approach has been chosen for the NCAR Climate System Model (*Boville and Gent* [1998]). Standardization of interfaces between atmospheric, oceanic, sea-ice, vegetation, ... models is a hard work which is the aim for example of the PRISM European project (*Ferraro et al.* [2003]).

Coming back to LMD5-CLIO2, the following sea-ice and ocean characteristics are provided by the OGCM to the AGCM:

1. sea-ice surface temperature,
2. sea-ice thickness,
3. sea-ice albedo,
4. sea-ice concentration,
5. sea-surface temperature,
6. ocean albedo.

The utility of these data are obvious for most of them, the only exception probably is the sea-ice thickness. The sea-ice thickness is needed to estimate the heat conduction through the sea-ice pack between atmosphere and ocean. Conversely, LMD5 transfers the following data to CLIO2:

1. sea-ice surface solar heat flux,
2. sea-ice surface non solar heat flux,
3. oceanic solar heat flux,
4. oceanic non solar heat flux,
5. snowfall,
6. surface freshwater budget (precipitation minus evaporation plus runoff),
7. runoff,
8. meridional and zonal wind stresses.

Again most of these data are obviously essential to compute the ocean and sea-ice evolution in the OGCM. The treatment of the water budget may seem strange. In fact, CLIO2 must be able to distinguish the snowfall from the net freshwater budget because a part of this kind of precipitation is trapped over sea ice and thus does not contribute directly to the oceanic surface freshwater budget. Furthermore, we want to be able to switch from the LMD5 Greenland runoff to the GISM[9] Greenland runoff. Hence, the continental runoff must be distinguished from the net freshwater flux. It is worth mentioning that no flux correction is employed.

The data exchanges between LMD5 and CLIO2 are orchestrated by a coupler, which performs the synchronization of the two models. All the fields mentioned above are transferred once a day. CLIO2 consumes much less CPU time than LMD5. Consequently, the oceanic model must wait the atmospheric at the end of each day. In fact, the coupler receives the fields sent by the ocean and transfers them to the atmosphere. Then, it receives the atmospheric fields and sends them to the ocean. The ocean waits until he receives these data. The coupler is based on the PVM software to perform all these data exchanges. Figure 2.9 gives the flow chart of LMD5-CLIO2. The coupler (in the center) starts. It enrolls into PVM, performs initializations, and spawns LMD5 (on the left) and CLIO2 (on the right), which in their turn start, enroll into PVM, and perform initializations. Both read boundary conditions, which are partly received once a day from the coupler. After the physical parameterizations, LMD5 sends average fields to the coupler once a day. They are interpolated by the coupler to the CLIO2 grid and sent to oceanic model at the beginning of the next day. CLIO2 uses them as boundary conditions and runs the dynamics and thermodynamics of sea ice and ocean. At the end of the day, sea-ice and oceanic surface characteristics are sent to the coupler. They are interpolated to the LMD5 grid and sent to the atmospheric model. And so on day after day. This description can give the impression that the coupling is asynchronous. In fact, both LMD5 and CLIO2 run at the same time: while LMD5 is running with the ocean and sea-ice surface features provided by CLIO2 at

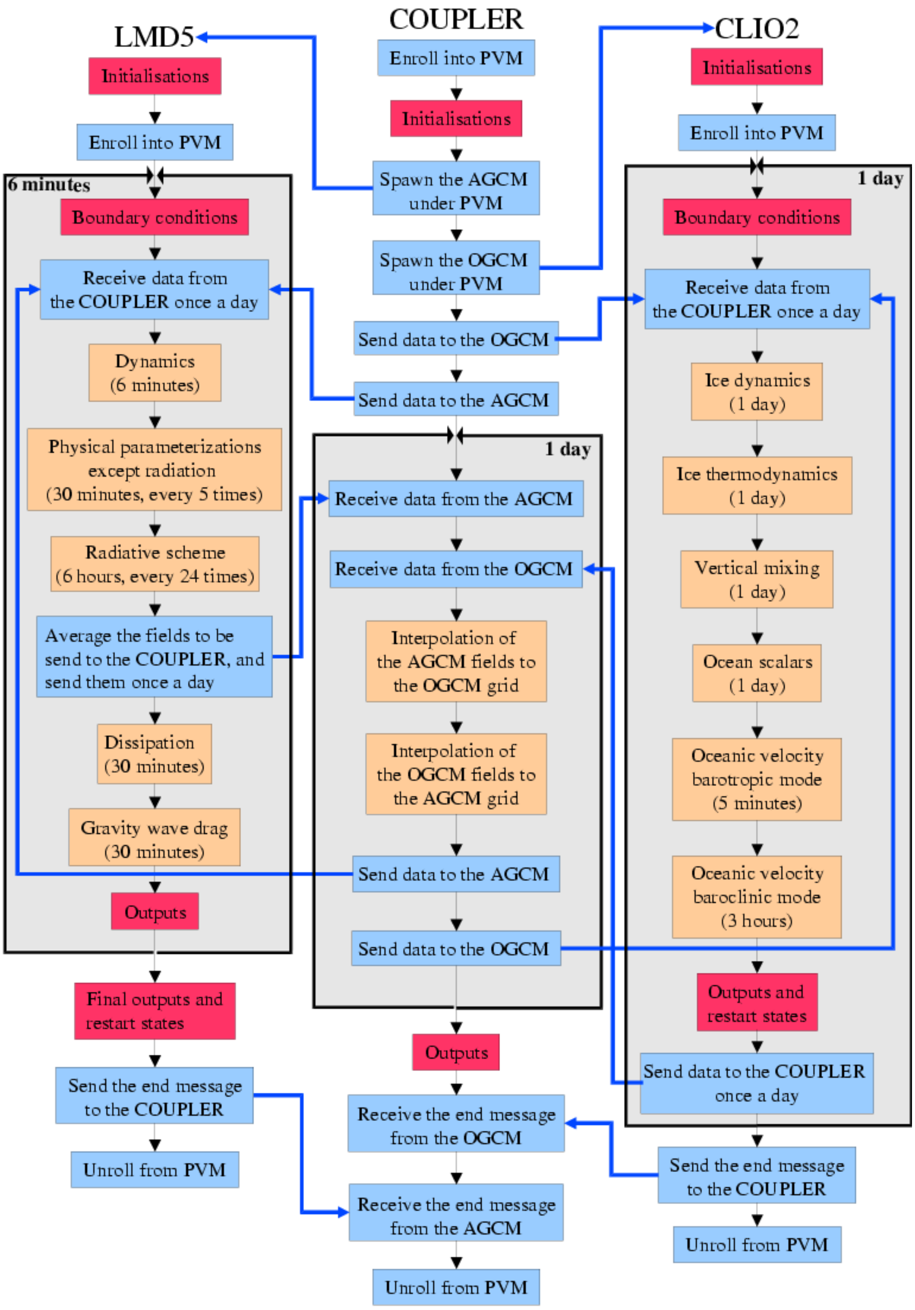

Figure 2.9: LMD5-CLIO2 flow chart. Our AOGCM is made of 3 programs: the atmospheric model LMD5 (on the left), the coupler (in the center) which orchestrates the data exchanges, the oceanic and sea-ice model CLIO2 on the right). The input/output parts are displayed in red. The PVM instructions are in blue. PVM is the software that is employed to perform the transfers between programs. The specific job of each program is in orange. A grey background accentuates the main loop of each program.

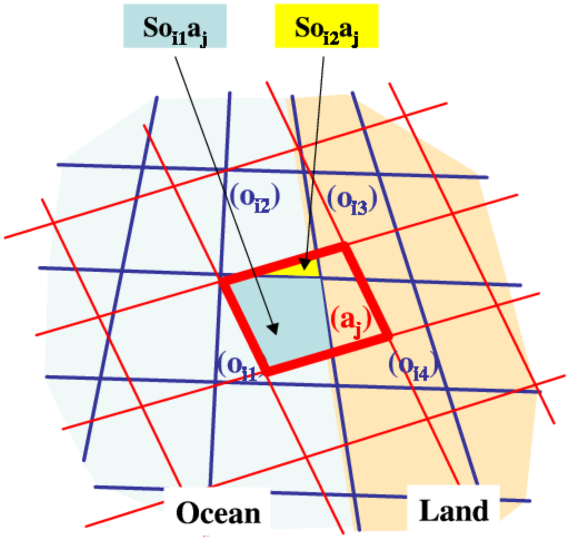

Figure 2.10: Conservative interpolation. The oceanic mesh is displayed by the blue lines, the atmospheric one is shown by the red lines. To obtain the value in an atmospheric grid (a_j), the values in the underlying oceanic grid cells are weighted according to the overlapping surfaces ($S_{o_{i1}a_j}$ in blue; $S_{o_{i2}a_j}$ in yellow). Furthermore, to adjust the AGCM continental mask to the OGCM one, the atmospheric grid a_j must contain an oceanic fraction equal to $S_{o_{i1}a_j} + S_{o_{i2}a_j}$ divided by the total grid area and a complementary land fraction.

the end of the previous day, CLIO2 is also running with the atmospheric fields received at the end of the previous day. It is a synchronous coupling method.

The main job of the coupler is to interpolate the transferred fields. The atmospheric and oceanic grids differ as explained in section 2.1.2. Subsequently, interpolation is requisite to transmit the fields from one grid to the other. From the atmosphere to the ocean, the interpolation must ensure the conservation of water and heat. An area-weighted approach has therefore been developed by *Grenier* [1995]. To obtain the value in an oceanic grid, the values in the overlying atmospheric grid cells are weighted according to the overlapping surfaces. By simplicity, the same method is used to interpolate oceanic fields on the the atmospheric grid as shown on figure 2.10. The interpolation scheme must also take into account the sea-ice fraction. Indeed, let's assume that an LMD5 grid cell overlies two oceanic grids, one (called A) without sea ice, one (called B) entirely covered by sea ice. The coupler indicates to the atmospheric grid cell that its sea-ice concentration should be 50 %. Consequently, LMD5 computes surface fluxes at the same time over ocean and over sea ice. At the end of the day, the coupler must transfer the oceanic fluxes to grid B and the sea-ice fluxes to grid A. The interpolation is thus based not only on overlapping surfaces but also on the sea-ice concentration. Subsequently, the weights used for this interpolation change every day. Finally, the coupling implies the interpolation of vectors, namely the surface stress. To avoid any problem with the vector direction, the surface stress is expressed in a fixed coordinate system located at the Earth's center. The three components are then interpolated and brought back to the local oceanic coordinate system.

Furthermore, the atmospheric continental mask has been adapted according to *Grenier* [1995] to fit the CLIO2 mask. To allow the adjustment of the LMD5 mask to the CLIO2 one, the atmospheric model has been adapted to permit coexistence of oceanic, continental, and sea-ice fractions in the same grid cell (figure 2.10). This modification is required to ensure water and energy conservations. It has been briefly described in section 2.1.5.6.

2.2 Greenland ice-sheet model

2.2.1 GISM overview

The Greenland ice-sheet model (GISM) consists of three main components which respectively describe the ice-sheet system, the solid Earth, and the surface mass balance. The latter of which represents the main driving force of the system. The GISM has been described in *Huybrechts et al.* [2002].

The ice-dynamics model (*Huybrechts et al.* [1991]) solves the fully coupled thermomechanical equations for ice flow on a high-resolution three-dimensional mesh. It takes into account the impact of internal deformation and basal sliding on the ice flow. The horizontal resolution of the model is of 20 km, and there are 31 layers in the vertical. The model is time-dependent and includes basal sliding and a temperature calculation within the bedrock. This basically involves the simultaneous solution of conservation laws for momentum, mass, and heat under appropriate simplifications, supplemented by Glen's flow law. The model has a free interaction between climatic input and ice thickness, and freely

[9] GISM is the Greenland ice-sheet model that has been coupled to LMD5-CLIO2 (see section 2.2).

generates the ice-sheet geometry in response to prescribed changes in sea level, surface temperature, and mass balance.

The mass balance model distinguishes between snow accumulation, rainfall, superimposed ice formation, and runoff, the components of which are all parameterized in terms of temperature. The melt-and-runoff model is based on the positive degree-day method and is similar to the method described in *Reeh* [1991]. It takes into account ice and snow melt, the daily temperature cycle, random temperature fluctuations around the daily mean, liquid precipitation, and refreezing of meltwater. The meltwater retention takes into account both the refreezing process and the capillary suction effect of the snow pack (*Janssens and Huybrechts* [2000]). Furthermore, the model calculates the fraction of precipitation falling as rain depending on the surface temperature, and treats the rainwater in a similar way as meltwater.

The bedrock model describes the interaction between changes in the ice loading and the bed elevation. In the model version that was applied for this work, a two-layer isostasy model is employed. In this approach, the time-dependent response of the bed depression is given by the viscous properties of the asthenosphere (upper mantle), which is overlain by a rigid elastic lithosphere that determines the ultimate shape of the imprint. Further details on the model can be found in *Huybrechts and de Wolde* [1999].

2.2.2 Coupling of LMD5-CLIO2 with GISM

GISM is coupled with LMD5-CLIO2 according to the scheme depicted in figure 2.11. This coupling is fully interactive and quasi-synchronous if one takes into account the large spread of model time steps, which are at maximum one year for the slowest model components (the ice sheet and its underlying bedrock).

The key atmospheric variables needed as input for GISM are surface temperature and precipitation. Because the details of the surface climate of Greenland are not well captured on the coarse LMD5 grid, these boundary conditions consist of a present-day component as represented on the much finer GISM grid to which climate change anomalies for LMD5-CLIO2 are superimposed. The present-day surface temperature over Greenland is parameterized as a function of latitude and surface elevation, and the current precipitation rate is prescribed from observations (see *Huybrechts et al.* [2002] for details). Temperature differences and precipitation ratios (climate change versus control) produced by LMD5-CLIO2 are interpolated from the LMD5 grid onto the GISM grid and respectively added or multiplied with the reference surface temperatures and precipitation rates. Temperature perturbations are applied monthly, but precipitation ratios are only imposed annually because reliable information on the monthly distribution of precipitation over Greenland is missing for the reference climate.

To couple GISM with LMD5-CLIO2, the ice-sheet model should be able to determine the annual freshwater fluxes feeding into the ocean. This involves the ice-sheet runoff, iceberg calving, runoff from the ice-free land, and melting below the ice sheet. The ice-sheet runoff is straightforwardly derived from the surface mass-balance model. The runoff from the tundra is set equal to the yearly precipitation. Calving dynamics and local ice shelves are not incorporated explicitly. Instead, the contemporaneous coastline acts as a natural barrier to grounded ice, beyond which all ice is transformed into calf ice. The

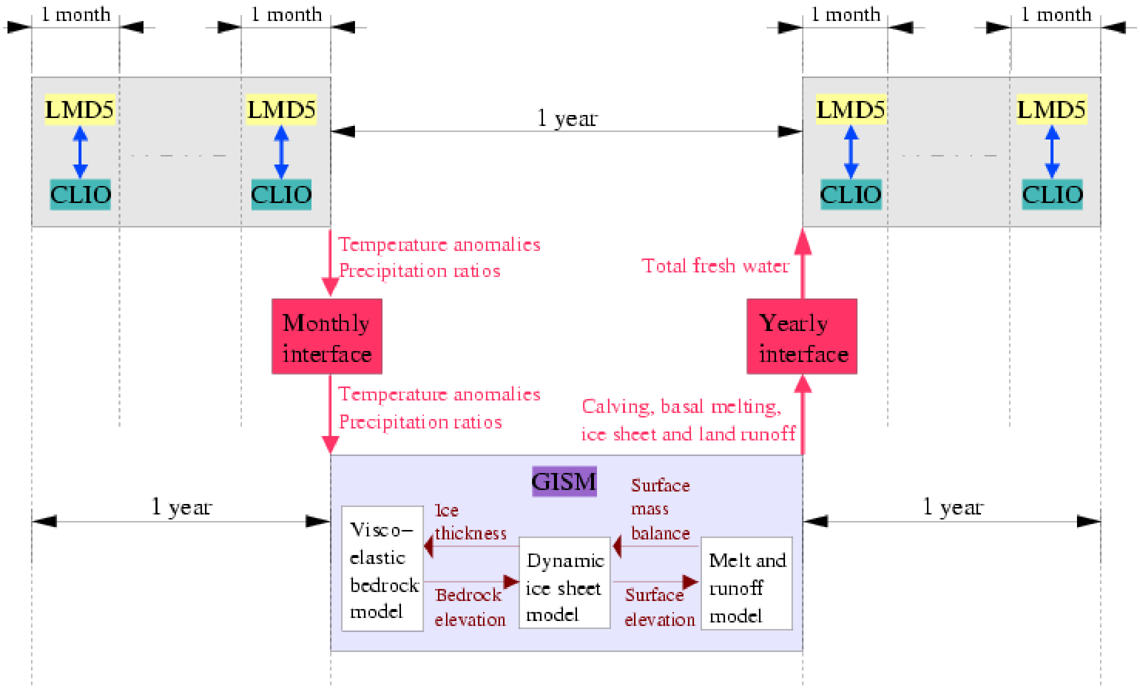

Figure 2.11: Coupling of LMD5-CLIO2 with GISM. The AOGCM flow chart has already been described in figure 2.9. LMD5 and CLIO2 run in parallel and exchange information every day. The AOGCM is integrated 12 times for 1 month. At the end of the year, monthly temperature anomalies and precipitation ratios are interpolated on the GISM grid and transfer (by files) to GISM. The ice-sheet model then performs a 1-year integration. The yearly averaged calving, basal melting ice-sheet runoff, and land runoff are computed by GISM. They are added up to get the total freshwater flux towards the ocean and distributed on the CLIO2 grid. This freshwater amount is divided by 12 to get monthly values.

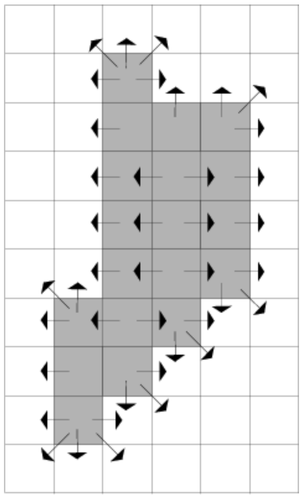

Figure 2.12: The GISM freshwater flux values are added up for each of the 19 grey grid cells (corresponding to the Greenland mask in CLIO2). Then, they are proportionally distributed into the adjacent oceanic CLIO grid cells according to the black arrows.

calving flux is thus calculated as the volume flux across the grounding line. Furthermore, a simple procedure was set up to allocate the total freshwater flux from the GISM to the respective oceanic grid boxes that border the Greenland continent (figure 2.12).

LMD5-CLIO2 does not accommodate for changes in the geometry of the Greenland ice sheet (elevation and extent) as these would be hardly detectable on the coarse atmospheric grid on a century time-scale. The ice dynamics model is only integrated forward after a net yearly surface mass balance has been established, meaning that the ice-sheet response and the associated freshwater fluxes are delayed by one year with respect to the climatic input. This is however not a serious problem considering the long response time-scales of the ice sheet and the ocean.

2.3 Experimental design

2.3.1 No flux correction

When AOGCM components are coupled, an initial drift occurs that brings the simulated climate away from observations. This behaviour is common to all AOGCMs, although its intensity differs (see *McAvaney et al.* [2001]). The basic reason is that nothing keeps the coupled model close to the observation unlike in forced mode when the model components are run separately. Indeed, AGCMs are forced by observed SST whatever surface fluxes they calculate, and OGCMs are forced by observed surface fluxes whatever SST they compute. So, even if the atmospheric and oceanic components succeed quite well in representing the observed climate, the coupled model may drift when the forcings are suppressed. Three elements combines to produce this drift:

- the fluxes provided by the atmosphere are not exactly those expected by the ocean;

- the surface characteristics provided by the ocean are not those used in forced mode by the atmosphere;
- the two components are not perfect, and errors arising in one component are often amplified by the other, as the surface fluxes and characteristics progressively change.

This adjustment phase is known as the "initial drift".

To restrain the drift, the scientific community exploits two leads. Firstly, the atmospheric fluxes computed by the AGCM are modified before being transferred to the OGCM. The adjustment fluxes are determined so that the coupled model remains close to the observations. This technique estimates the systematic errors in the model fluxes and adapts their atmospheric estimation to what the oceanic model would expect. These flux corrections are determined from previous simulations and remains fixed during the whole coupled run. Consequently, in climate change simulations, the AOGCM is "free" to move to a perturbed climate. This first attempt to restrain the coupled model drift has several drawbacks. On the one hand, the overimposed flux corrections do not have any physical background. They can not be adapt to different climatic conditions. Nothing indicates that their use is advisable under different climatic conditions. For example, the adjustment flux amplitude may be as large as, or larger than the net observed flux along the sea-ice margin. This enables the corrected model to keep sea ice in grid cells where no sea ice would be simulated otherwise. Under warmer atmospheric conditions, this flux correction is unrealistic if the sea-ice margin moves polewards. Furthermore, flux correction can modify the model sensitivity. For example, the correction near the sea-ice margin will delay the disappearance of sea ice in those grid cells. To sum up, the arbitrary adjustment fluxes can change the model mean state but also its variability.

The second lead follows by the scientific community is to improve the model components and puts up with "small" drifts. This is a long and exacting task. Model parameters have to be tuned in forced mode but also in coupled mode (which is CPU-time consuming) as the AOGCM behaviour can differ from the AGCM or OGCM ones. Improved parameterizations have to be developed based on a more accurate representation and understanding of the underlying physical processes. The model resolution must also be improved.

This second approach has been chosen for this work. No flux correction is used. The main goal is to perform climate change experiments. The disadvantages explained above convince us to make this choice. Nevertheless, no new parameterizations have been tested. That was far over the scope of this thesis. Parameters have been adapted as mentioned in sections 2.1.5, 2.1.3, 2.1.4 in the LMD5 or CLIO2 models.

2.3.2 Initial conditions

Another key element is the choice of the initial conditions, which influence the initial drift. As the time scales involved in the oceanic processes are long (more than one thousand years for the deep ocean), the coupled model requires long integration to get to equilibrium. On the more powerful computers available for this work (a Compaq Alpha ES40), about 7 CPU hours are required to simulate 1 year; i.e., 290 days are required to simulate such a thousand-year simulation with the coupled model. This is of course impossible. Different approaches have been imagined and tested within the coupled model community, with the common goal of restraining the computer cost. Sometime, the AGCM and OGCM are separately using surface conditions or fluxes computed asynchronously by the other component. For example, the atmospheric model can be run for 5 years (reasonable time scale to reach equilibrium) with surface characteristics from an equilibrium state of the OGCM under observed conditions. The surface fluxes computed by the AGCM are stored. Then the OGCM is run for a thousand years using those fluxes. And so on. This method spares CPU time as the most consuming model (usually the AGCM) is integrated for a short period. Nevertheless, the equilibrium state reached this way can differ from the one that would be obtained by a fully coupled simulation. Consequently, an initial drift can persist when coupling the two models. More complex approaches have been developed that also imply fully coupled periods in these "spin-up" runs.

We opt to a simple "spin-up". LMD5 is run to equilibrium in forced mode by a 5-year simulation. CLIO2 is integrated to a quasi-equilibrium state. A thousand-year simulation has been performed in forced mode under present observed conditions. The end states of both simulations are in reasonable agreement with the observed climate, but some biases are already present. This choice concerning the initial states is based on the following assumption: these biases would by any way appear in LMD5-CLIO2 as they arise from model deficiencies. We decide to get them in forced mode for two reasons. Firstly, it is less time consuming to get them in forced mode than in coupled mode. Secondly, in forced mode, the model deficiencies can not bring the results far from the observed climate, whereas nothing ensures this in coupled mode as more feedbacks can amplify errors. One can bring up against this that the impact of the model weaknesses would perhaps have been different in coupled mode.

Similarly, GISM has been first run during the last two glacial-interglacial cycles up to the year 1970 with forcing from ice-core data to derive initial conditions for coupling with LMD5-CLIO2 (see *Huybrechts and de Wolde* [1999] for details). The length of this run is linked to the long response time-scale of the Greenland ice sheet.

2.3.3 Forcings

The aim of this thesis is to estimate the impact of increasing levels of the greenhouse gas and sulphate aerosol concentrations in the atmosphere on the Earth's climate. Thus, the forcing is the greenhouse gas concentration and the sulphate aerosol loading. A scenario is used for the 21st century that takes into account the forecasted evolution of the emissions. The IPCC published new emission scenarios in 2000 (*Nakićenovic et al.* [2000]). As these experts say:

> " Future greenhouse gas emissions are the product of very complex dynamic systems, determined by driving forces such as demographic development, socio-economic development, and technological change (...) A set of scenarios was developed to represent the range of driving forces and emissions in the scenario literature so as to reflect current understanding and knowledge about underlying uncertainties. "

Four preliminary marker scenarios were provided as input for climate models. Most modeling groups decided to use only two of them for the Third Assessment Report published

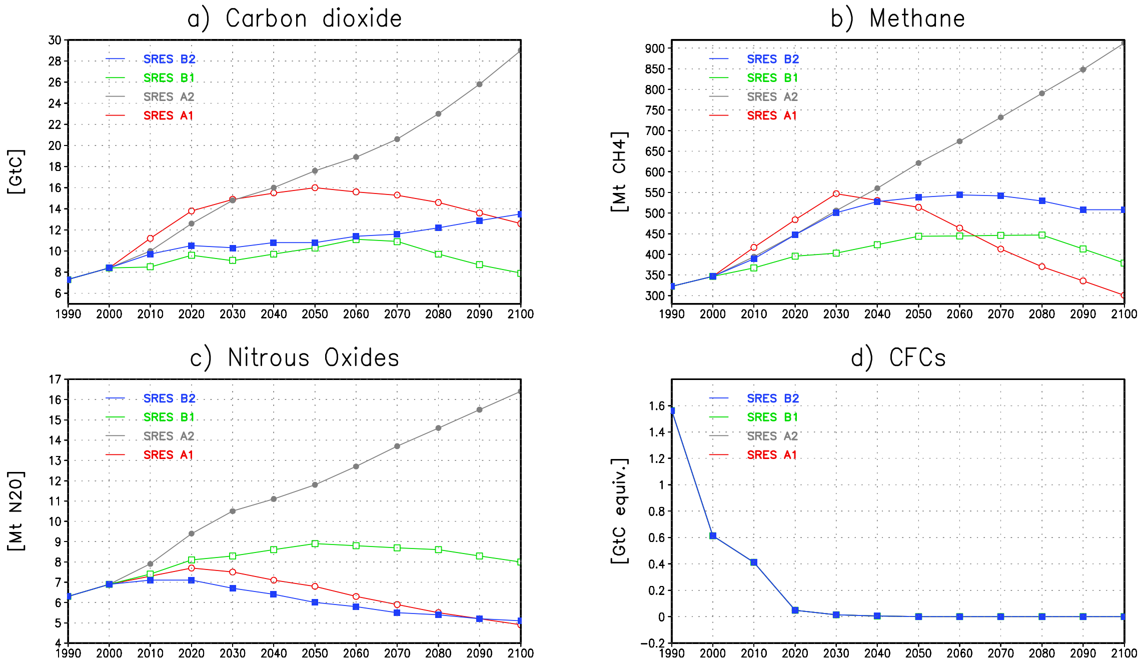

Figure 2.13: Greenhouse-gas emission scenarios from the IPCC report (*Nakićenovic et al.* [2000]). The preliminary marker scenarios of the 4 storylines are displayed for carbon dioxide (a), methane (b), nitrous oxides (c), and CFCs (d).

by the IPCC in 2001, the so-called SRES A2 and B2 storylines. The A2 storyline describes a very heterogeneous world where the main theme is self-reliance and preservation of local identities. Global population increases continuously and technological change are slow. This leads to relatively high greenhouse gas emissions. The B2 storyline describes a world in which the emphasis is on local solutions to economic, social and environmental sustainability. While the scenario is oriented towards environmental protection and social equity, it focuses on local and regional levels. The greenhouse gas emissions are smaller than in the A2 storyline but higher than in the most optimistic storylines where global solutions to economic, social, and environmental sustainability is assumed. Due to time limitation, only one of these two scenarios has been run once with LMD5-CLIO2, and once with LMD5-CLIO-GISM. We choose the SRES B2 marker scenario as it leads to intermediate greenhouse gas emissions (figure 2.13).

The emission scenarios are transformed through models describing the atmospheric chemistry, the atmosphere-ocean interaction, ... toward atmospheric concentration projections. As the greenhouse gases are well mixed in the atmosphere, no geographical distribution pattern is needed. Figure 2.14 shows the CO_2, CH_4, N_2O, $CFC-11$, and $CFC-12$ concentrations for the SRES B2 scenario used in the climate change simulations.

The sulphate aerosol loading and its effect on the shortwave radiation absorbed at the top of the atmosphere is displayed in figure 2.15 for 1970 and for the projection in 2099 according to the SRES B2 scenario. The sulphate aerosols remain during a short period in the atmosphere. Consequently, the aerosol loading is not uniform over the Earth. The

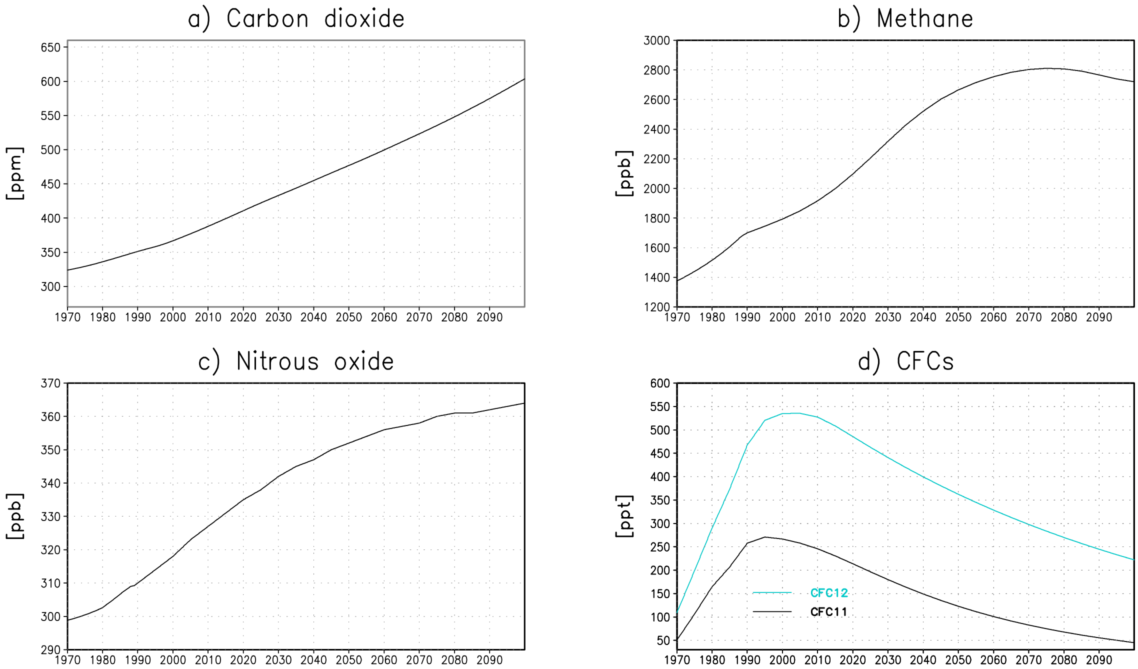

Figure 2.14: Time evolution of the CO_2, CH_4, N_2O, $CFC-11$, $CFC-12$ atmospheric concentration projected for the SRES B2 marker scenario.

loading is greater over regions of strong emission. The model that provided us with the geographical distribution of the sulphate aerosol loading is described in *Chuang et al.* [1997] and *Penner et al.* [1998]. Monthly values were provided for 1965, 1980, 1990, 2010, 2030, 2050, 2070, and 2100. Linear interpolation over time was performed to get data for other years. Data were of course not on the LMD5 grid. Subsequently, a spatial interpolation has been developed. It is based on a overlapping area-weighted average.

Two climate change experiments have been performed (figure 2.16): one with fixed freshwater flux from the Greenland (called hereafter SRESb2), one with freshwater flux computed by GISM (called hereafter SRESb2G). The runoff and calving adopted in the SRESb2 simulation comes from the preliminary run performed with the Greenland ice-sheet model over the last two glacial-interglacial cycles (section 2.3.2). It provides us with a simulated 1970 freshwater flux from Greenland which was in reasonable agreement with the observational data available.

To get rid of the model drift in the estimation of climate change, a control run is performed. Its results are subtracted to the climate change experiment values. This has to be seen as a first attempt to eliminate the drift. Nevertheless, nothing ensures that the drift is identical in both simulations.

The control simulation (called hereafter CONT) is the reference for climate change simulations (SRESb2 and SRESb2G). Due to computer cost and time delay, this work does not deal with climate change observed during the 20th century. It does not tackle the problem of detection and attribution over that period as defined by the IPCC report (*Houghton et al.* [1996]) (see chapter 1). Indeed, to perform such a study, a control run

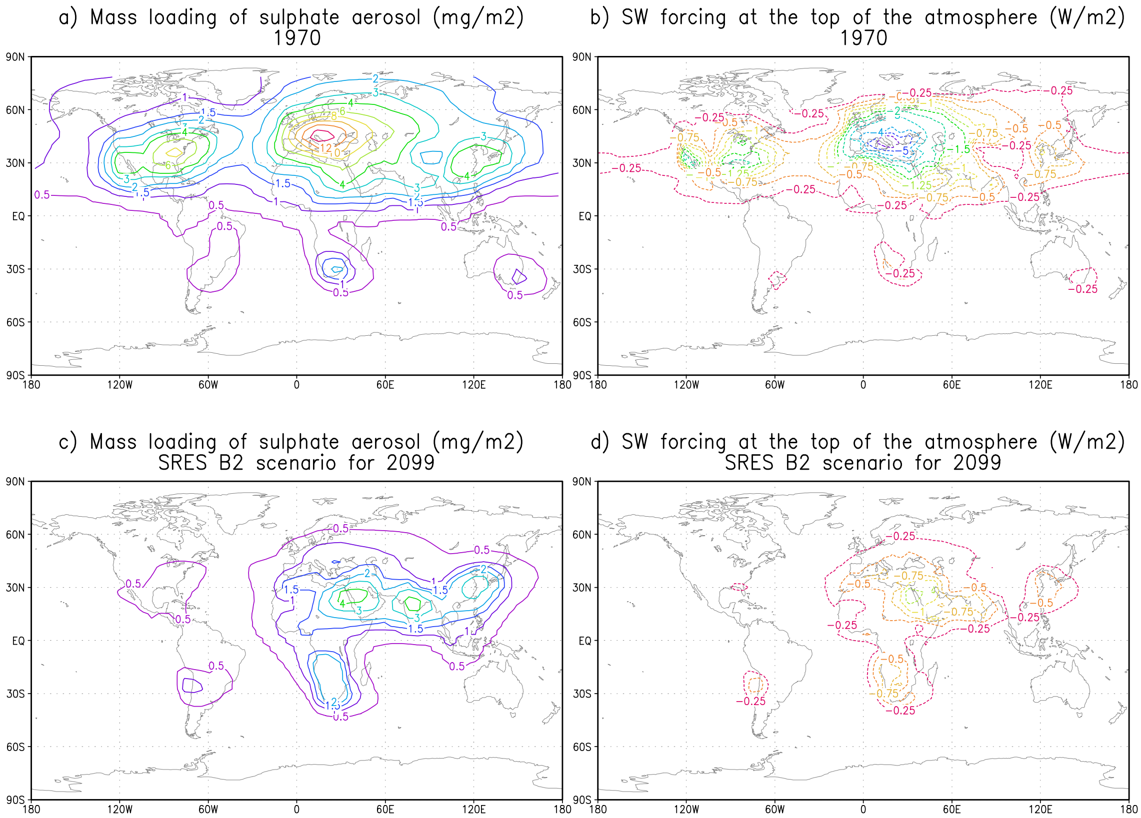

Figure 2.15: Aerosol loading and its impact on the net shortwave radiation at the top of the atmosphere forecasted by the SRES B2 scenario for 2099 (c,d). The 1970 values are also shown (a,b).

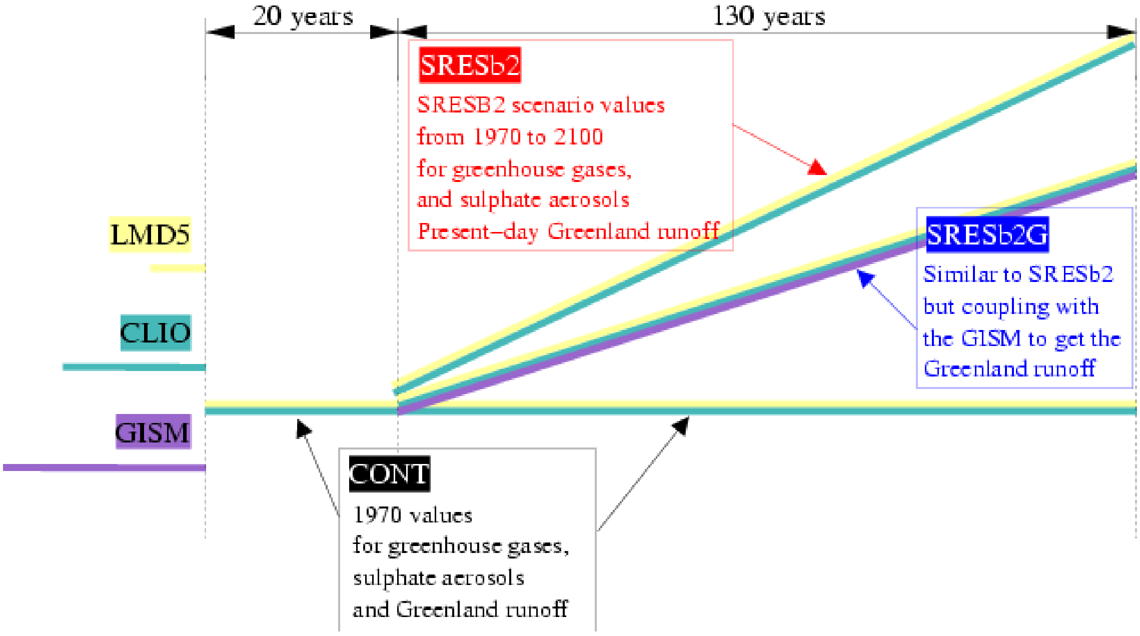

Figure 2.16: Experimental design. Preliminary forced runs have been performed with LMD5, CLIO2, and GISM. The control run (CONT) then starts with LMD5-CLIO2. At year 20 of CONT, two climate change simulations begin: one without GISM (SRESb2) and one with GISM (SRESb2G).

starting at pre-industrial period (1765) is necessary. This would lead to a 335-year simulation. This is much too long for the computer power available (it would require about 100 CPU days). Furthermore, the control simulation uses constant forcings. The greenhouse gas concentrations are kept constant during the whole run. Moreover, the impact of volcano and solar constant modifications are not included in our simulations.

If the model is not integrated from the quasi-equilibrium pre-industrial state, the warming induced by greenhouse gases is delayed. This is known as the cold start effect. When the climate change experiment starts, the model is at equilibrium which "present-day" forcing conditions. It does not simulate the warming due to previous amplification of the greenhouse effect. *Fichefet and Tricot* [1992] have shown that 1970 is a good compromise to limit the impact of the cold start effect. Therefore, the greenhouse gas and sulphate aerosol concentrations are prescribed to their 1970 values in the CONT simulation. The geographical pattern of sulphate aerosol loading for 1970 is shown in figure 2.15a,b. The greenhouse gas concentrations are: 323.774 $ppmv$ for carbon dioxide CO_2, 1374.99 $ppbv$ for methane CH_4, 298.82 $ppbv$ for nitrous oxide N_2O, 50.5 $pptv$ for CFC-11, and 108.9 $pptv$ for CFC-12. The Greenland runoff is kept constant throughout the CONT experiment to the 1970 values provided by the GISM preliminary run.

2.3.4 Experimental design

To sum up, the CONT simulation starts from quasi-equilibrium states of the forced LMD5 and CLIO2 models. LMD5-CLIO2 is directly run in fully-coupled mode without any flux

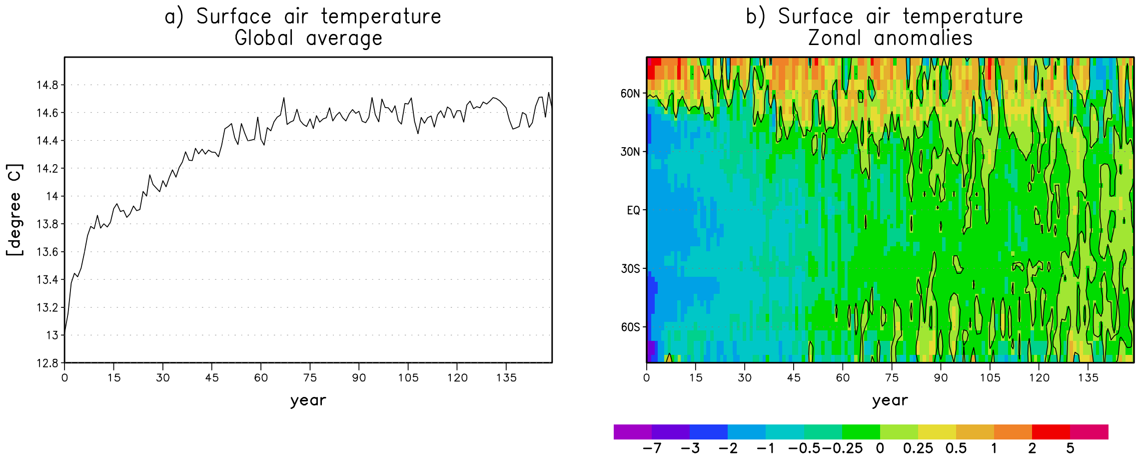

Figure 2.17: Time evolution of the surface air temperature (°C) during the 150 years of the CONT simulation. (a) global mean, (b) zonally averaged difference between the surface air temperature and its value at the end of the simulation ("end" means average over the last 30 years of the run).

correction. As a rapid drift occurs during the first years (see section 2.4), the climate change experiments SRESb2 and SRESb2G start at year 20 of the CONT simulation. GISM was previously run over the two last glacial-interglacial cycles. This provides us with an initial state. The SRESb2 and CONT simulations are LMD5-CLIO2 simulations using constant runoff and calving from Greenland (the initial state values). The SRESb2G experiment is performed by LMD5-CLIO2 and GISM in fully coupled mode. This set of simulations allowed us to project climate changes and to estimate the impact of the Greenland ice sheet on the climate during the 21st century. The CONT simulation is 150-year long. The SRESb2 and SRESb2G experiments cover the end of the 20th century and the whole 21st century (1970 to 2100).

2.4 Drift in the CONT experiment

The first step of this thesis has been devoted to the reduction of the LMD5-CLIO2 drift. As already said, many sensitivity experiments were performed to atmospheric, oceanic or sea-ice parameterizations. The chosen values for the involved parameters are given in sections 2.1.3, 2.1.4 and 2.1.5). Here, only the final experiment, which is the CONT simulation, is analyzed.

Prior to the analysis of the present-day climate simulated by LMD5-CLIO2 (chapter 3), the model drift is described in this section. The time evolution of surface air temperature and precipitation illustrate the atmospheric evolution. To complete this information, the global averages of sea-surface temperature (SST) and oceanic temperature are computed and displayed for the 150 years of the CONT simulation. Then, the variation of the sea-ice volume and effective area is drawn. Finally, the maximum overturning in the North Atlantic Ocean indicates a reduction of the thermohaline circulation.

On a global average, the air at the surface of the Earth increases by about 1.6°C during

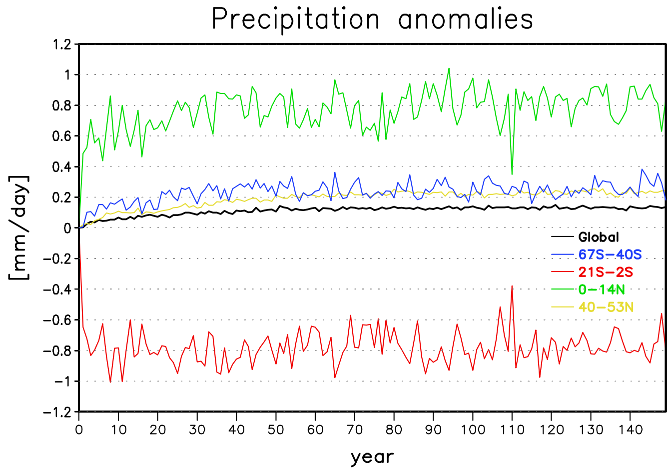

Figure 2.18: Precipitation evolution during the CONT simulation. This graph shows the difference with the first year of the simulation for various regions. (black curve) global mean, (blue curve) from about 67°S to 40°S, (red curve) from about 21°S to 2°S, (green curve) from about 0° to 14°N, (yellow curve) from about 40°N to 53°N.

the 150 years of the CONT simulation as shown in figure 2.17a. A rapid warming occurs during the 10 first years. Then, the drift slows down. After about 50 years, the remaining drift is very small. To get further information on this drift, the time evolution of the difference with the temperature at the end of the simulation is drawn in figure 2.17b for each latitude. During the first 5 years, the surface air is obviously colder than at the end. This leads to negative values at most latitudes except in the Northern Hemisphere high latitudes. The total drift (from the beginning to the end of the CONT simulation) can reach about 7°C near Antarctica. This warming is associated to a strong reduction of the sea-ice extent (see below). The amplitude of the warming is reduced towards the equator, slightly more than 1°C in the intertropical region. The Northern Hemisphere mid-latitudes warm by about 2°C from the beginning to the end of the CONT simulation. On the contrary, the high latitude temperature is about 4°C higher at year 1 than at the year 150. The cooling reaches 15°C in the Barents and Kara Seas which are invaded by sea ice in the first few years. From 40°N to 90°N, the end of the simulation is characterized by a cold period. This end cooling does not seem significant as the interannual variability is high during the whole run. In general, most of the drift is finished after 50 to 70 years. The interannual variability decreases towards the equator.

Globally averaged precipitation increases (figure 2.18, black curve), especially during the first 50 years of the CONT experiment. This global amplification of the hydrological cycle is consistent with the global warming simulated during this simulation. The largest modifications occur in the intertropical regions. Southwards of the equator (red curve in figure 2.18), precipitation is reduced. This decrease is mainly localized over the western Pacific Ocean in the Warm Pool, whose temperature diminishes. On the contrary, precipitation increases northward of the equator (green curve in figure 2.18). Again, most changes take place over the Pacific Ocean. Smaller intensification of precipitation is also observed in the Southern Hemisphere mid-latitudes (blue curve in figure 2.18) over the Southern

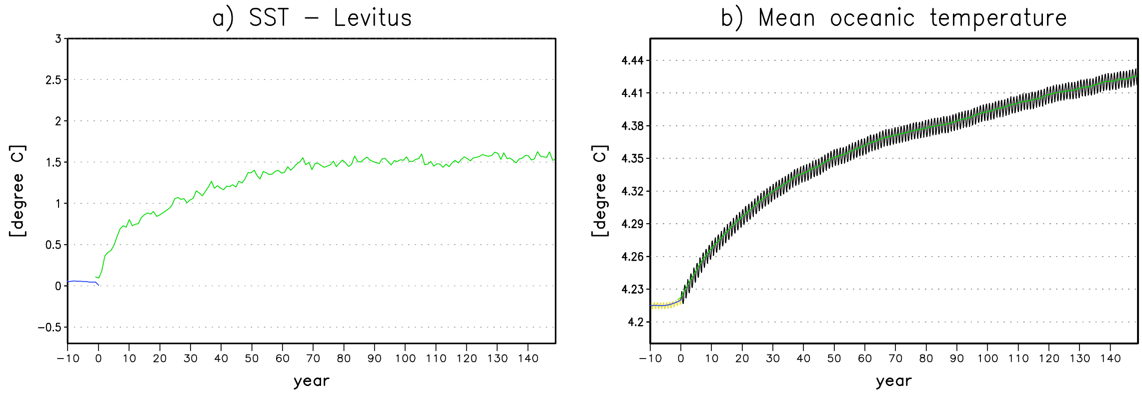

Figure 2.19: Time evolution of (a) global mean sea-surface temperature minus the Levitus' climatology values (*Levitus* [1982]), (b) global mean oceanic temperature integrated over the whole oceanic depth. The black and yellow curves show the seasonal cycle, the annual mean values are plotted in green and blue. The CONT simulation starts in year 0 and ends in year 150 (green and black curves). Previous values (yellow and blue curves) come from the CLIO2 simulation in forced mode that provides us with the initial state for the CONT run, there are thus displayed before year 0.

Ocean and in the Northern Hemisphere mid-latitudes (yellow curve in figure 2.18) over the oceans. The intertropical drift is very quick, most of it occurs within the first 10 years of the simulation. Its amplitude reaches $+0.8$ mm/day in the Northern Hemisphere and -0.9 mm/day in the Southern Hemisphere. Then, much slower changes happen.

The sea-surface temperature imitates the evolution of the surface air temperature. The sea-surface warming gets to 1.4°C at the end of the simulation (figure 2.19a), slightly lower than the surface air warming of 1.6°C. Most of the temperature increase occurs during the first 50 years of the CONT simulation. Afterwards, the remaining drift equals $\frac{0.33°\mathrm{C}}{100\ \mathrm{years}}$. Deeper in the ocean, the warming is slower. The time scale of the bottom water renewal is a few thousand years. Subsequently, the temperature in the ocean interior does not reach an equilibrium at the end of the simulation (figure 2.19b). After an stronger initial drift, it stabilizes at $\frac{0.077°\mathrm{C}}{100\ \mathrm{years}}$.

In the Northern Hemisphere, the sea-ice effective area increases rapidly during the first 20 years (figure 2.20a). The initial state, coming from the CLIO2 run in forced mode, has an annual mean sea-ice effective area of about 11.5×10^6 km^2. This variable rapidly goes up to 13.8×10^6 km^2 at year 20. Afterwards, no significant drift is simulated. Modification of the seasonal cycle is even quicker. The amplitude of the seasonal cycle of about 10.8×10^6 km^2 in forced mode is reduced to 7.6×10^6 km^2 after one year of coupled simulation and remains almost constant afterwards. Similarly, the Arctic sea-ice volume increases during the first 20 years (from 28.8×10^3 km^3 in the CLIO2 forced simulation to 49.5×10^3 km^3 at year 20). The volume is not as stable as the sea-ice effective area. The annual mean sea-ice volume oscillates between about 43×10^3 km^3 and 51×10^3 km^3 during the last 130 years of the CONT experiment.

Around Antarctica, sea ice rapidly melts (figure 2.20b): from an annual mean sea-ice effective area of 13.5×10^6 km^2 in the CLIO2 run, only 2.5×10^6 km^2 persists at year 10.

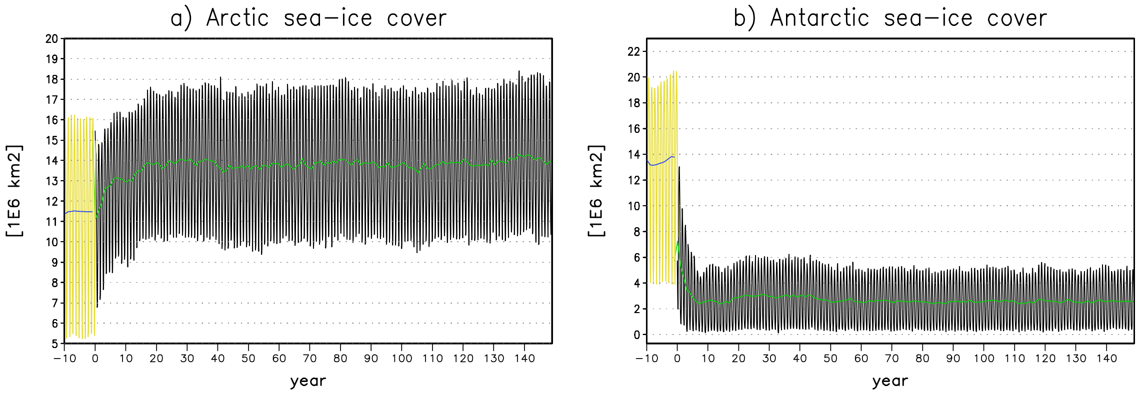

Figure 2.20: Time evolution of (a) Northern Hemisphere sea-ice effective area, (b) Southern Hemisphere sea-ice effective area. The black and yellow curves show the seasonal cycle, the annual mean values are plotted in green and blue. The CONT simulation starts in year 0 and ends in year 150 (black and green curves). Previous values (yellow and blue curves) come from the CLIO2 simulation in forced mode that provides us with the initial state for the CONT run, there are thus displayed before year 0.

This decreases of the annual mean is mainly due to a strong underestimation of the sea-ice cover in winter: only $5.5 \times 10^6\,\mathrm{km}^2$ instead of $19 \times 10^6\,\mathrm{km}^2$ in forced mode. The summer values rapidly decreases to very low values (about $0.25 \times 10^6\,\mathrm{km}^2$) as sea ice remains only in the Weddell and Ross Seas. Like the sea-ice extent, the sea-ice volume shows the impact of the intense initial melting. CLIO2 simulates an annual mean sea-ice volume of about $12.6 \times 10^3\,\mathrm{km}^3$ which seems reasonable. But LMD5-CLIO2 can not keep such a big sea-ice volume (only $2.5 \times 10^3\,\mathrm{km}^3$ remains at year 10).

The thermohaline circulation does not reach equilibrium by the end of the CONT simulation. A drift is present throughout the CONT run. To illustrate this, the time evolution of the North Atlantic Deep Water overturning strength[10] is plotted in figure 2.21. The decrease rate seems to be reduced at the end of the control simulation: it is about 0.12 Sv/yr during the first 80 years and 0.04 Sv/yr over the last 70 years[11].

The climate change experiments start from year 20 of the CONT simulation. At the sight of these results, it would seem more appropriate to waited until year 50 because most surface drifts become very small afterwards. This retrospective view was impossible as the CONT and climate change experiments have been achieved at the same time. Between the first attempt to start the CONT simulation on the computers and its completion, about 2.5 months have elapsed. It was not possible to wait such a long time to begin the other experiments.

[10] computed as the maximum of the annual mean meridional streamfunction in the North Atlantic Ocean.
[11] $1\,Sv = 10^6\,m^3 s^{-1}$

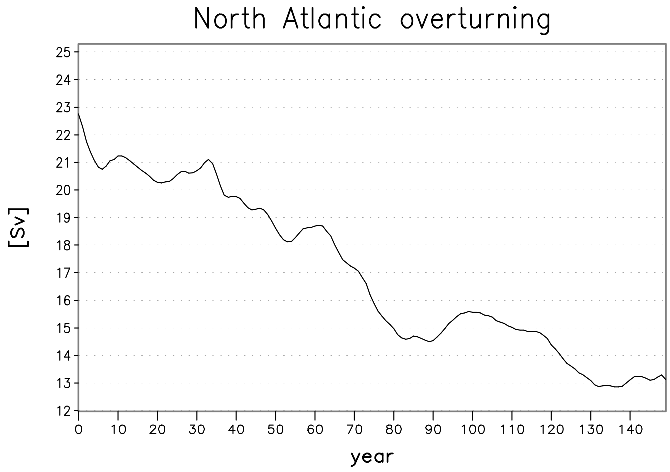

Figure 2.21: Time evolution of the NADW overturning strength (Sv) during the CONT experiment.

2.5 Conclusion

A first version of the LMD-CLIO coupled model had been developed at the Institut d'Astronomie et de Géophysique G. Lemaître (UCL) by H. Grenier and M. El Mohajir (*Grenier* [1997]). It has been improved during this thesis work to enable longer realistic simulations over the 21st century. Some modifications aimed to reduce the initial drift of this non-flux corrected model: introduction of a new formulation of the horizontal advection of water vapour, adaptation of atmospheric parameters, improved version of the CLIO2 model, transfer of new oceanic and sea-ice fields from CLIO2 to LMD5. Other developments were made within the context of climate-change experiments: a new radiative scheme has been included which accounts separately for each greenhouse gas, the direct sulphate aerosol effect has been parameterized through changes of the surface albedo.

Nevertheless, when the LMD5-CLIO2 model is integrated using constant 1970 forcings (the CONT simulation), it progressively departs from observations. At high latitudes, most of the temperature drift takes place during the first 10 years: (a) a partial disappearance of sea ice around Antarctica associated to surface temperature overestimation, (b) a strong cooling in the Barents, Kara and GIN Seas rapidly invaded by sea ice. The surface air temperature trend is much smaller in other regions and most of the drift is confined in the first 50 years. Afterwards a small residual drift remains. Similar initial drifts occur in other non-flux corrected models.

To get such a reasonable 150-year long simulation, a lot of sensibility simulations were performed to investigate the impact of various parameters. As a first step, LMD5-CLIO2 was integrated for short 10-year simulations to restrain the rapid initial drift. Secondly, longer runs were achieved to investigate the reason of the slower drift. In a first 170-year integration, it turns out that the version of LMD5-CLIO2 was enable to maintain a realistic thermohaline circulation. A mistake was found in the continental runoff scheme which accounts twice for the snowfall. It led to overestimation of the continental runoff into the Arctic basin. The freshening of the surface water improved the vertical stability in the ocean. Consequently, the Barents, Kara and GIN Seas were rapidly invaded by sea ice. Afterwards, a surface freshwater tongue spreads into the North Atlantic ocean leading to a shutdown of the deep convection in this region around year 70. After this first attempt, the CONT simulation has been achieved with an improved version of LMD5-CLIO2. Although the intensity of the North Atlantic thermohaline circulation decreases during the 150 years of the simulation. The deep water formation remains active and the North Atlantic overturning is close to 13 Sv at the end of this run, an intensity similar to the one obtained with other non-flux corrected AOGCMs.